The University of Tennessee
Department of Mechanical and Aerospace Engineering

ANALYSIS OF THE VISCO SEAL
PART II
THE CONCENTRIC TURBULENT CASE

by
William K. Stair
Robert H. Hale

Investigation conducted for the
National Aeronautics and Space Administration
under
Research Grant NsG-587

June 28, 1966
Knoxville, Tennessee

N66-32803

ABSTRACT

This report, the seventh of a series, presents a theoretical analysis of the visco seal when operating in turbulent flow. The general approach taken was to modify the Navier-Stokes equations for use in turbulent flow. Using an approach similar to that of S. I. Pai, the velocity profile in the seal was represented as a power series and a solution of the resulting flow equations resulted in an equation for the sealing coefficient suitable for laminar or turbulent flow.

An approximate method has been devised wherein the friction data for ordinary pipe flow can be utilized to determine the experimental factors in the sealing equation. From the experimental study of ten seal geometries it was observed that the agreement between theory and experiment was quite satisfactory for purposes of seal design.

Author

TABLE OF CONTENTS

LIST OF TABLES

LIST OF FIGURES

NOMENCLATURE

A	Area, in.
a	Axial land width, in.
b	Axial groove width, in.
C_1, C_2	Terms in equation 11
C_3, C_4	Experimental coefficients in equation 17
C_5-C_{20}	Constants of integration
c	Radial clearance, in.
D	Seal diameter, in.
$E = \left[1 + 1.5\epsilon^2\right]$	Eccentricity factor in equation 14
$F.P = \frac{4\pi}{Re_c} \Phi$	Friction parameter
f	Resistance coefficient, Figure 5
h	Groove depth, in.
$h_g = h + c$	Film thickness over grooves, in.
$j = b \cos \alpha$	Groove width, in.
$j' = a \cos \alpha$	Land width, in.
L	Active seal length, in.
l	Axial threaded length of seal, in.
M	Exponent in equation 70
M'	Exponent in equation 71
N	Exponent in equation 58
N'	Exponent in equation 59
n	Number of thread starts
n	Exponent in equation 17
P	Instantaneous pressure, lbf./in.^{2}
$\overline{P}$	Time averaged pressure, lbf./in.^{2}
P'	Turbulent fluctuating pressure, lbf./in.^{2}
$\overline{P}_1$	Pressure at $\xi^* = 0$, $\eta^* = 0$, and $z^* = -1$, lbf./in.^{2}
Q	Sealant flow rate, in.^{3}/sec.
q	Power loss, in. lbf./sec.

$Re_c = \frac{Uc\rho}{\mu}$	Reynolds number based on clearance
S.C. ( )	Theoretical sealing coefficient as presented in Chapter I. Letter in brackets refers to author.
s	Thread pitch, in.
s^*	Thread pitch per thread, in.
T	Time, sec.
$t = \tan \alpha$	Tangent of the helix angle
U	Surface velocity of the seal, in./sec.
u,v,w	Instantaneous velocity component in the ξ, η, and z directions, in./sec.
$\bar{u},\bar{v},\bar{w}$	Time averaged velocity component in the ξ, η, and z directions, in./sec.
u',v',w'	Turbulent fluctuating velocity component in the ξ, η, and z directions, in./sec.
x	x coordinate in the direction of motion
y	y coordinate along shaft axix
z	z coordinate in the radial direction
α	Helix angle, degrees
$\beta = \frac{h + c}{c}$	Dimensionless parameter
$\gamma = \frac{b}{a + b}$	Dimensionless parameter
δ	Half thickness between parallel plates, in.
ϵ	Eccentricity ratio
η	η coordinate
Λ	Sealing coefficient as presented in this work
μ	Absolute viscosity, lbf. sec./in.^{2}
ξ	ξ coordinate
ρ	Density, lbf. sec.^{2}/in.^{4}
τ	Wall shearing stress, lbf./in.^{2}
Φ	Dissipation function

Subscripts

c	Denoting evaluation on clearance
ct	Denoting Couette flow
$\mathcal{C}$	Denoting centerline
E	Denoting experimental
g	Denoting grooves
h	Denoting film thickness
h_g	Denoting film thickness over grooves
$\mathcal{l}$	Denoting laminar flow
o	Denoting turbulent flow
P	Denoting Poiseuille flow
p	Denoting pipe Reynolds number
r	Denoting lands
T	Denoting theoretical
η	Denoting η direction
ξ	Denoting ξ direction

Superscript

*	Denoting non-dimensional term

CHAPTER I

INTRODUCTION AND ANALYTICAL HISTORY OF THE VISCO SEAL

I. INTRODUCTION

The visco seal, which has been referred to in literature as screw seal, spiral groove seal, threaded seal, viscosity pump, and viscosity seal, is a rotating device which will develop a pressure gradient in the fluid annulus around a shaft by means of helical grooves located either on the shaft or in the housing. The basic elements of a visco seal are shown in Figure 1. Since there is normally no contact between the rotating shaft and the housing, the visco seal has been considered for use in critical apparatus which require long life, such as liquid metals systems in space power plants and pumps and compressors in nuclear power reactor systems as well as in various pumps, compressors, and turbines in more conventional systems. The increased interest in visco seal application in both the aerospace and basic industries was the impetus for this work.

Analytical work on the visco seal has been limited primarily to the laminar flow case. The means of predicting the operation of the visco seal in the turbulent region has been, in the main, empirical. The object of this study is to develop a theory for predicting the performance of the visco seal when operating in the turbulent range, and to determine the correlation between the theory developed and experimental evidence obtained for a number of seal geometries.

II. HISTORICAL PRESENTATION OF LAMINAR VISCO SEAL ANALYSES

The first notable laminar analysis of the visco seal was presented by Rowell and Finlayson [1] [1] in 1928. Starting with the Navier-Stokes equations for two-dimensional incompressible flow and assuming the clearance between the screw and housing to be zero, Rowell and Finlayson developed an equation for the discharge from a visco pump which neglected the effects

---

[1] Numbers in brackets refer to similarly numbered references listed at the end of this report.

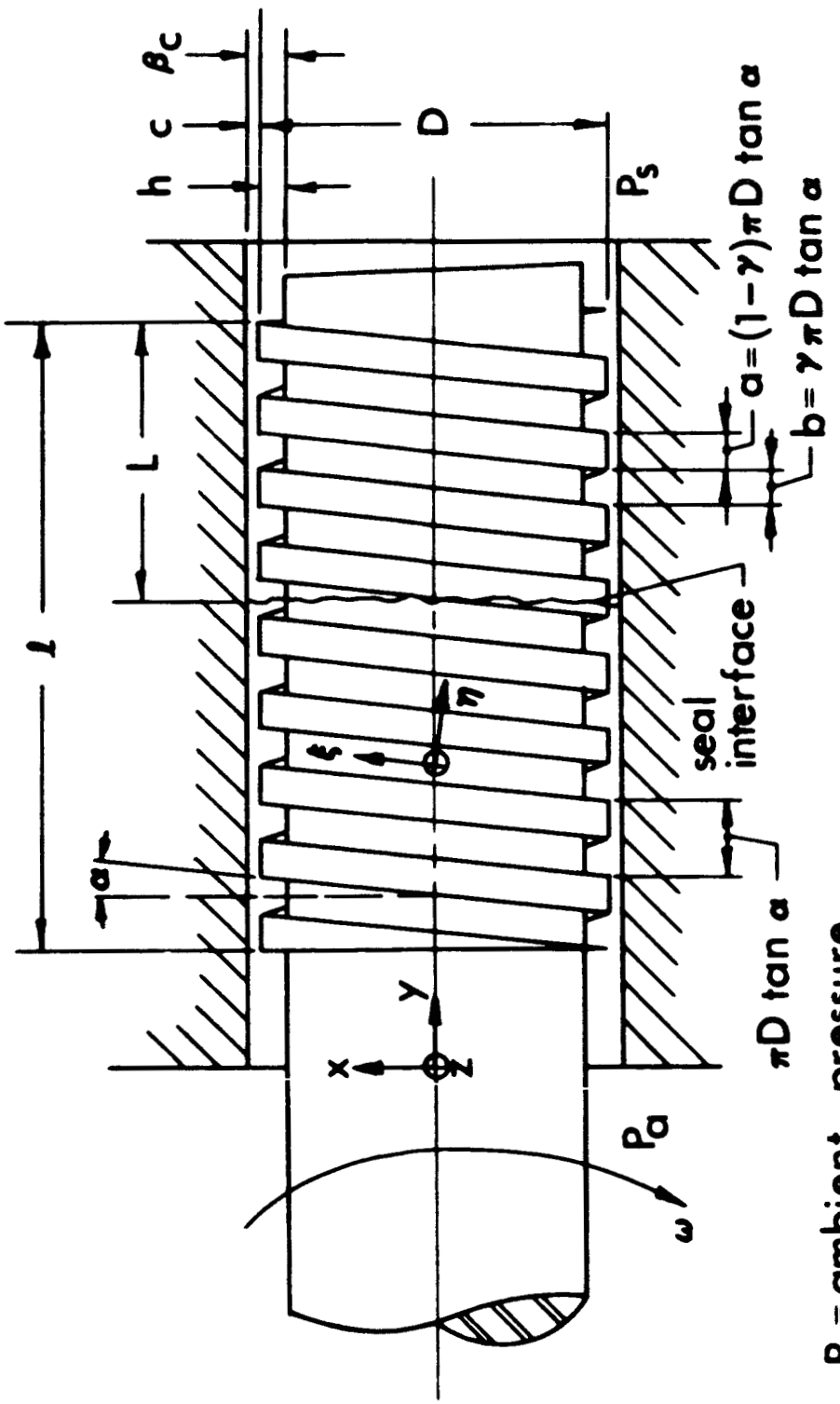

Figure 1. Basic elements of the visco seal.

of the screw helix angle, α. This equation is:

$$Q = 2j^2 \left[\frac{4U}{\pi^3} \sum_{i=1}^{\infty} \frac{\sinh \frac{i\pi h}{j}}{i^3 \left(\cosh \frac{i\pi h}{j} + 1\right)} - \frac{jh\Delta P}{24\mu L} + \frac{8j^2 \Delta P}{\pi^5 \mu L} \sum_{i=1}^{\infty} \frac{\sinh \frac{i\pi h}{j}}{i^5 \left(\cosh \frac{i\pi h}{j} + 1\right)} \right] . \quad (1)$$

Equation (1) was believed to be suitable for visco pumps having a small helix angle. When the helix angle was large enough to be significant, Rowell and Finlayson recommended that the discharge be evaluated as:

$$Q = \frac{2s^2 \cos^2 \alpha}{\left(1 + \frac{a}{b}\right)^2} \left\{ \frac{8U \cos \alpha}{\pi^3} \sum_{i=1}^{\infty} \frac{\tanh \frac{i\pi h}{2j}}{i^3} - \left[\frac{h}{12j} - \frac{16}{\pi^5} \sum_{i=1}^{\infty} \frac{\tanh \frac{i\pi h}{2j}}{i^5} \right] \left[\frac{2s^2 \cos^2 \alpha \sin \alpha}{\left(1 + \frac{a}{b}\right)^2} \frac{\Delta P}{\mu L} \right] \right\} . \quad (2)$$

While Rowell and Finlayson were considering the device as a pump which could obtain a theoretical maximum efficiency of 33.33 per cent, they envisioned the visco pump being operated at shut off head or no-flow condition, thus becoming a visco seal. Setting the discharge equal to zero and defining a sealing coefficient, equation 2 becomes:

$$S.C._{(R.F.)} \equiv \frac{6\mu UL}{\Delta P}$$

$$= \frac{\frac{3}{2} \pi^3 j^2 \tan \alpha \left[\frac{h}{12j} - \frac{16}{\pi^5} \sum_{i=1}^{\infty} \frac{\tanh \frac{i\pi h}{2j}}{i^5} \right]}{\sum_{i=1}^{\infty} \frac{\tanh \frac{i\pi h}{2j}}{i^3}} . \quad (3)$$

$i = 1, 3, 5, \ldots$

It is noted that the sealing coefficient in equation 3 depends upon the groove depth, groove width, and helix angle, but does not distinguish between laminar and turbulent operation. Thus, the sealing pressure developed would be a linear function of the shaft speed. Rowell and Finlayson considered the geometry of the grooves in regard to their effect on the pump performance but did not attempt to establish an optimum seal geometry.

Whipple [2] developed a theory for the pressure distribution and load capacity for a herringbone type thrust bearing. His equations can be transformed to apply to the present seal geometry. The equation for the sealing coefficient based on Whipple's work becomes:

$$S.C._{(w.)} \equiv \frac{6\mu UL}{\Delta Pc^2}$$

$$= \frac{(\beta^3 + 1) + 2\beta^3 \left[\frac{1 - 2\gamma(1-\gamma)}{\gamma(1-\gamma)}\right] + (\beta^3 - 1)^2 \cos 2(90 - \alpha)}{(\beta^3 - 1)(\beta - 1) \sin 2(90 - \alpha)} \quad . \qquad (4)$$

Whipple determined the optimum geometry, giving a minimum value of the sealing coefficient as 10.96, resulting when $\beta = 3.61$, $\gamma = 0.5$, and $\alpha = 13.75°$. Hughes [3] utilized the results of Whipple's equation in constructing a visco seal and experimentally showed that the sealing pressure came within 12 per cent of the theoretical value predicted by equation (4).

Zotov [4] assumed the flow to consist of three components: the annulus flow parallel to the shaft axis due to the pressure gradient, the flow along the grooves caused by the pressure gradient, and the flow along the grooves due to the rotation of the shaft. The three flow components were identified as: land pressure flow,

$$Q_r = m \frac{4\pi D \Delta Pc^2 (a + b)}{\mu L} \quad , \qquad (5)$$

groove pressure flow

$$Q_g = k \quad \frac{\pi D \Delta P j h^2 \tan\alpha \sin\alpha}{12 \mu L (a + b)} \quad , \tag{6}$$

and groove rotational flow,

$$Q_g = \frac{\pi D U h j \sin\alpha}{2 (a + b) \left(\frac{h}{j} + 1\right) \left[1 + \left(\frac{4h}{j} + 1\right) \frac{c}{h}\right]} \quad , \tag{7}$$

where the factors m and k are given by:

$$m = 5.31 \times 10^{-3} \left(\frac{a}{c}\right)^{-0.75}$$

and

$$k = 1 - 0.63 \left(\frac{a}{c}\right)$$

when $0 < \frac{a}{c} < 0.8$. Combining equations (5), (6), and (7) to form the total flow, and setting this quantity equal to zero, which represents the condition of sealing, the sealing coefficient becomes:

$$S.C._{(Z_1)} = \frac{6 \mu U L}{c^2 \Delta P}$$

$$= \left(\frac{h}{j} + 1\right)\left[1 + \left(\frac{4h}{j} + 1\right) \frac{c}{h}\right]\left[\frac{k \tan\alpha}{\left(\frac{c}{h}\right)^2} + \frac{48m \left(\frac{a + b}{j}\right)^2}{\frac{h}{j} \sin\alpha}\right] \quad . \tag{8}$$

Equation (8) is a function of groove width, land width, helix angle, groove depth, and clearance. Equation (8) does not, however, take into account turbulence. As the rotational speed increases, Zotov's theoretical sealing coefficient, like Rowell and Finlayson's and Whipple's, will remain constant. Optimizing Zotov's equation produces a sealing coefficient of 8.69 for a screw geometry of $\gamma = 0.63$, $\alpha = 14.5°$, and $\beta = 4.12$.

One of the earliest reports in which experimental data are recorded either for a visco pump or a visco seal operating in the turbulent region was presented by Frossel [5]. Limited analytical work is

incorporated in this paper which is primarily devoted to reporting experimental data for the various screw threads tested. Frossel uses an equation developed by Gumbel to describe the discharge from the visco pump as:

$$Q = \frac{n\,j\,h}{2}\left(U\cos\alpha - \frac{h^2}{6\mu}\frac{dP}{d\xi}\right) \quad . \tag{9}$$

In developing equation (9), Gumbel assumed one dimensional flow along the grooves only. Thus equation (9), written in terms of the sealing coefficient, becomes:

$$S.C._{(G.)} \equiv \frac{6\mu UL}{\Delta P} = h^2 \tan\alpha \tag{10}$$

Frossel concludes that for a visco pump the trapexoidal thread shapes are the most practical, since they have the largest flow cross-section with the lowest fricitional loss. Frossel notes in his discussion that as the shaft speed was increased, discontinuities occurred in the data which were attributed to turbulence. Frossel made no attempt, however, to predict the point where turbulence occurs or how the visco pump should behave during turbulent operation.

Asanuma [6] analyzed the performance of the visco pump by considering the pump delivery to be composed of two parts: actual delivery and flow leakage. Asanuma's equation for the sealing coefficient was:

$$S.C._{(A.)} \equiv \frac{6\ \ UL}{c^2\,\Delta P} = \frac{\beta^3\gamma(1-\gamma)\,C_1\sin^2\alpha + 1}{\beta\,\gamma(1-\gamma)\,C_2\sin\alpha\cos\alpha} \quad , \tag{11}$$

where

$$C_1 = \left(\frac{\beta-1}{\beta}\right)^2 - \frac{8\beta^2}{\pi^4}\left(\frac{c}{a}\right)\sum_{i=1}^{\infty}\left\{\frac{1}{i^4}\sin\frac{i\pi}{\beta}\left[\cos\frac{i\pi}{\beta} - (-1)^i\right]\tanh\right.$$

$$\left.\frac{i\pi}{2\beta}\left(\frac{a}{c}\right)\right\} \quad . \tag{12}$$

and

$$C_2 = \frac{(\beta - 1)^2 (\beta + 2)}{\beta^3} + \frac{3}{\beta^2} \left[C_1 - \left(\frac{\beta - 1}{\beta} \right)^2 \right]$$

$$- \frac{48\beta}{\pi^5} \left(\frac{c}{a} \right) \sum_{i=1}^{\infty} \frac{1}{i^5} \left[\cos \frac{i\pi}{\beta} - (-1)^i \right]^2 \tanh \frac{i\pi}{2\beta} \left(\frac{a}{c} \right) . \qquad (13)$$

In equation (11) the sealing coefficient is a function of groove width and depth, clearance, land width, and helix angle, but is independent of rotational speed. Asanuma suggests that the best sealing coefficients will be obtained for $\gamma = 0.5$, $\alpha = 10°$ to $11°$ and $\beta = 6.0$.

McGrew and McHugh [7] reported experimental data obtained from tests in both laminar and turbulent operation and presented an analytical solution for the sealing performance under laminar conditions. McGrew and McHugh, following the work of Zotov, assumed that the total flow in the pump is comprised of three main components: a flow due to shear, a minus pressure flow in the grooves, and a negative leakage flow. The equation for the total flow in the pump becomes:

$$Q = \frac{n h U (s^* - a) \cos^2 \alpha}{2 \left(1 + \frac{c}{h} \right)} - \frac{n h^3 (s^* - a) \cos \alpha \sin \alpha \Delta P}{12 \mu L}$$

$$- \frac{E \pi D s c^3 \Delta P}{12 \mu n a L} . \qquad (14)$$

Setting equation (14) equal to zero, McGrew and McHugh's sealing coefficient becomes:

$$S.C._{(M.M.)} \equiv \frac{6\mu UL}{c^2 \Delta P} = \frac{(\beta - 1)^3 \gamma \beta t^3 (1 - \gamma) + E\beta (t^2 + 1)}{(\beta - 1)^2 \gamma t (1 - \gamma)} . \qquad (15)$$

where

$$E = 1 + 1.5\epsilon^2$$

The theoretical sealing coefficient in equation (15) is a function of clearance, groove depth, groove and land widths, helix angle, and eccentricity ratio but is independent of speed. Minimizing the sealing coefficient, equation (15) produces a sealing coefficient of 9.83 for $\gamma = 0.5$, $\alpha = 21.6°$, and $\beta = 3.78$. For the turbulent analysis of the visco seal McGrew and McHugh employed a Prandtl mixing length type of solution, and expressed the axial pressure gradient in terms of three experimentally determined factors. The equation which best fits McGrew and McHugh's data, and the one used to describe operation in the turbulent region is:

$$S.C._{(M.M.)_o} \equiv \frac{6\mu UL}{c^2 \Delta P} = 6 \left[0.313 + 1.31 \times 10^{-4} \, Re_h^{\,1.044} \right]^{-1} . \qquad (16)$$

The empirical factors in equation (16) were obtained from the data for a single screw geometry and affords no provision for a change in seal geometry.

A recent source of data for the operation of the visco seal in turbulent flow was published by King [8] who used the equation,

$$S.C._{(K.)} \equiv \frac{6\mu UL}{c^2 \Delta P} = 3 \left[C_3 + C_4 \, Re_{hg}^{\,n} \right]^{-1} , \qquad (17)$$

developed by McGrew and McHugh. King fits equation (17) to his experimental data and can therefore determine the experimental constants.

The analytical solution which appears to best describe the laminar operation of the visco seal was presented by Boon and Tal [9]. Stair [10], whose laminar analysis of the seal parallels Boon and Tal's, both refines and expands the equations developed by Boon, arriving at a sealing coefficient of:

$$S.C._{(S.)} \equiv \frac{6\mu_U L}{c^2 \Delta P} = \frac{\beta^3 (1 + t^2) + t^2 \gamma (1 - \gamma) (\beta^3 - 1)^2}{t \gamma (1 - \gamma) (\beta^3 - 1) (\beta - 1)} . \quad (18)$$

Equation (18) is dependent on land and groove width, groove depth, clearance, and helix angle. Optimizing equation (18) results in a sealing coefficient of 10.97 for a seal having $\gamma = 0.5$, $\beta = 3.65$, and $\alpha = 15.68°$.

III. COMPARISON OF LAMINAR ANALYSES FOR THE VISCO SEAL

A comparison of the laminar analyses for the visco seal is presented in Figure 2. All theories are compared using the same geometrical screw configuration of $\gamma = 0.63$, $\beta = 3.38$, and $\alpha = 14.5°$. The sealing coefficients in Figure 2 were computed as

$$\frac{6 \mu_U L}{c^2 \Delta P},$$

which required modification of some equations in order to gain a common ground for comparison. Rowell and Finlayson's and Gumbel's equations, both of which were derived neglecting the leakage flow across the lands, appear to be considerably in error, while the predictions of McGrew and McHugh ($\epsilon = 0$), Zotov, Whipple, Asanuma, and Boon and Tal compare more favorably with the experimental values.

The approach taken in this work will be to extend Boon and Tal's laminar analysis for the sealing coefficient of the visco seal to both laminar and turbulent operation.

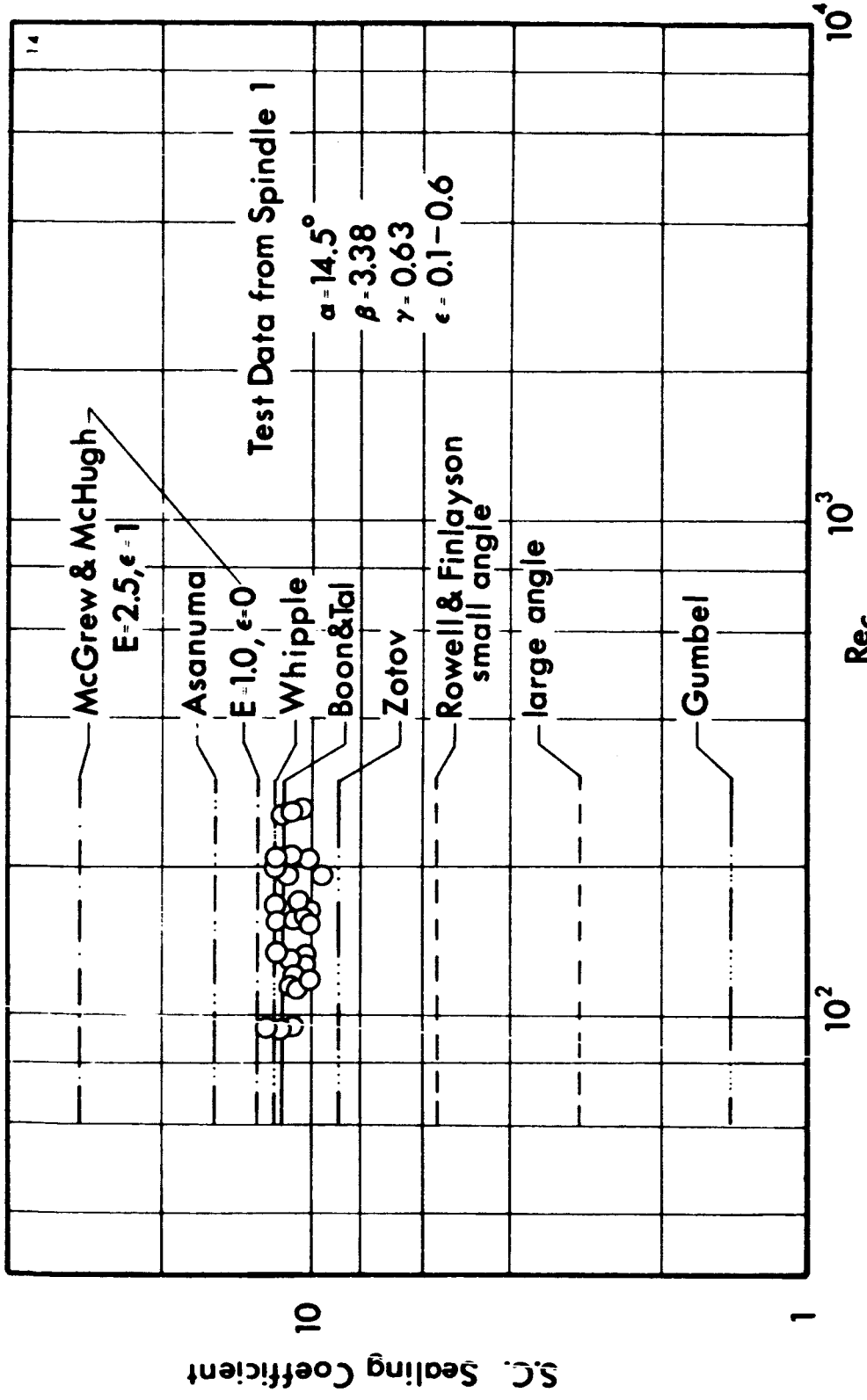

Figure 2. Comparison of laminar test data and analytical theories for the visco seal.

CHAPTER II

DEVELOPMENT OF THE SEALING COEFFICIENT

I. BASIC FLOW EQUATIONS

In analyzing the flow in the visco seal it will be assumed that the film thickness is small as compared to the radius. Hence, neglecting the curvature of the seal the problem reduces to the one shown in Figure 3. It is noted, however, that for small diameter shafts and high rotational speeds this assumption becomes less valid due to the centrifugal acceleration of the fluid. The basic describing equations will be written in the ξ , η , and z coordinates and later transposed to the x, y, and z coordinates. The two sets of coordinate axes are related by:

$$\xi = \cos\alpha + y \sin\alpha \tag{19}$$

and

$$\eta = y \cos\alpha - x \sin\alpha \quad . \tag{20}$$

The Navier-Stokes equations for a Newtonian fluid, neglecting body forces and assuming that the flow is incompressible, steady, and laminar, are:

$$\rho\left[u\frac{\partial u}{\partial \xi} + v\frac{\partial u}{\partial \eta} + w\frac{\partial u}{\partial z}\right] = -\frac{\partial P}{\partial \xi} + \mu \nabla^2 u, \tag{21}$$

$$\rho\left[u\frac{\partial v}{\partial \xi} + v\frac{\partial v}{\partial \eta} + w\frac{\partial v}{\partial z}\right] = -\frac{\partial P}{\partial \eta} + \mu \nabla^2 v, \tag{22}$$

and

$$\rho\left[u\frac{\partial w}{\partial \xi} + v\frac{\partial w}{\partial \eta} + w\frac{\partial w}{\partial z}\right] = -\frac{\partial P}{\partial z} + \mu \nabla^2 w \, . \tag{23}$$

The law of continuity requires that:

$$\frac{\partial u}{\partial \xi} + \frac{\partial v}{\partial \eta} + \frac{\partial w}{\partial z} = 0. \tag{24}$$

To apply equations (21) through (24) to turbulent flow, the instantaneous velocity component may be considered to contain two parts: the mean velocity component and the turbulent fluctuating component. This concept can also be applied to the pressure. Therefore:

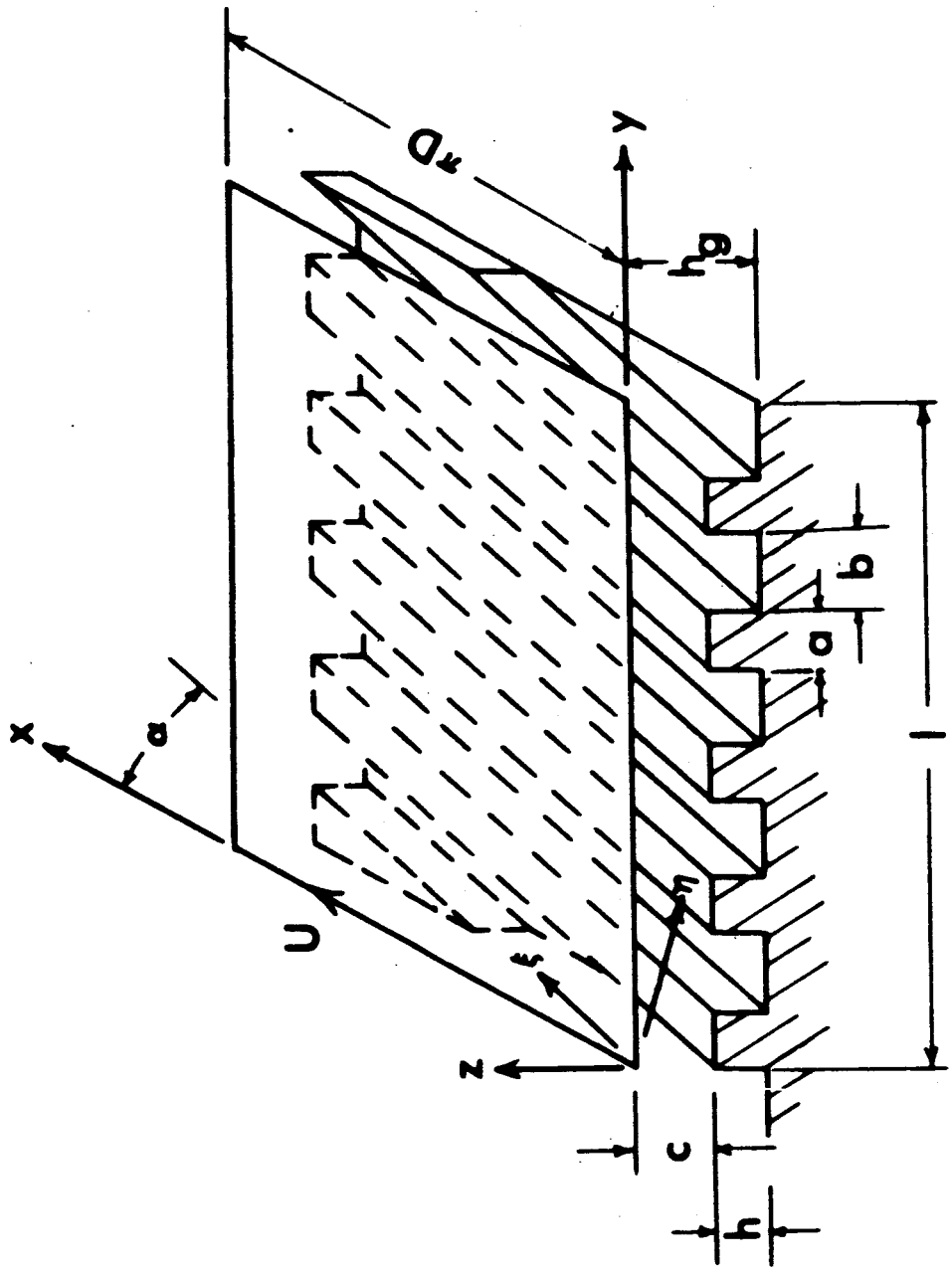

Figure 3. Developed view of the visco seal geometry.

$$u = \bar{u} + u' , \tag{25}$$

$$v = \bar{v} + v' , \tag{26}$$

$$w = \bar{w} + w' , \tag{27}$$

and

$$P = \bar{P} + P' . \tag{28}$$

Using equations (25) through (28) in equations (21) through (24) and time averaging and combining equations (21) through (24), the Reynolds equations, as reported by Pai [11], are formed. Hence:

$$\rho\left[\bar{u}\frac{\partial \bar{u}}{\partial \xi} + \bar{v}\frac{\partial \bar{u}}{\partial \eta} + \bar{w}\frac{\partial \bar{u}}{\partial z}\right] = -\frac{\partial \bar{P}}{\partial \xi}$$

$$+ \mu \nabla^2 \bar{u} - \rho\frac{\partial \overline{u'^2}}{\partial \xi} - \rho\frac{\partial \overline{u'v'}}{\partial \eta} - \rho\frac{\partial \overline{u'w'}}{\partial z} , \tag{29}$$

$$\rho\left[\bar{u}\frac{\partial \bar{v}}{\partial \xi} + \bar{v}\frac{\partial \bar{v}}{\partial \eta} + \bar{w}\frac{\partial \bar{v}}{\partial z}\right] = -\frac{\partial \bar{P}}{\partial \eta}$$

$$+ \mu \nabla^2 \bar{v} - \rho\frac{\partial \overline{u'v'}}{\partial \xi} - \rho\frac{\partial \overline{v'^2}}{\partial \eta} - \rho\frac{\partial \overline{v'w'}}{\partial z} , \tag{30}$$

and

$$\rho\left[\bar{u}\frac{\partial \bar{w}}{\partial \xi} + \bar{v}\frac{\partial \bar{w}}{\partial \eta} + \bar{w}\frac{\partial \bar{w}}{\partial z}\right] = -\frac{\partial \bar{P}}{\partial z}$$

$$+ \mu \nabla^2 \bar{w} - \rho\frac{\partial \overline{u'w'}}{\partial \xi} - \rho\frac{\partial \overline{v'w'}}{\partial \eta} - \rho\frac{\partial \overline{w'^2}}{\partial z} . \tag{31}$$

In equations (29) through (31), all three turbulent fluctuating velocity components are assumed to be of the same order of magnitude. Noting that Δz is small as compared to $\Delta\xi$ and $\Delta\eta$ and assuming $\bar{w}$ is negligible with negligible pressure change in the z direction, the Reynolds equations become:

$$\frac{\partial \bar{P}}{\partial \xi} = \mu \frac{\partial^2 \bar{u}}{\partial z^2} - \rho \frac{\partial \overline{u'w'}}{\partial z} \quad , \tag{32}$$

and

$$\frac{\partial \bar{P}}{\partial \eta} = \mu \frac{\partial^2 \bar{v}}{\partial z^2} - \rho \frac{\partial \overline{v'w'}}{\partial z} \quad . \tag{33}$$

Equations (32) and (33) are the describing differential equations which will be applied to the visco pump and later simplified for the visco seal.

II. BASIC FLOW EQUATIONS APPLIED TO THE CONDITIONS OF THE VISCO PUMP

In a screw pump, since $a \gg c$ and $b \gg h_g$, the flow is approximated by assuming that it resembles flow between two sets of flat plates: one set of plates being separated by the distance c, the other by h_g. In defense of this assumption, it should be noted that in a visco pump the order of magnitude of a and b is approximately 100 to 1000 that of c and h_g respectively. The problem now simplifies to that shown in Figure 4. The flow equations will be developed in a general form and the results applied to both the grooves and the lands.

In order to acquire a solution for equations (32) and (33) as applied to a visco pump two parameters are required: the mean velocity distribution and a relationship for the turbulent wall shear, τ_o. The approach taken in this work, therefore, is similar to the one used by Pai, in which the velocity distribution for turbulent flow was approximated with a power series. An approximation of this nature is required since a functional relationship between $\overline{u' w'}$ and z and $\overline{v' w'}$ and z does not exist. Pai analyzed the problem of turbulent flow between parallel plates for two cases. The first case consisted of the top plate moving with the bottom one fixed, or turbulent Couette flow. In the second case the flow is due to a pressure gradient, or turbulent Poiseuille flow. In the visco pump both types of flow exist. While equations (32) and (33) are non-linear and do not lend themselves to the principal of superposition, the approximations used for the mean velocity profile are well behaved convergent series. Therefore,

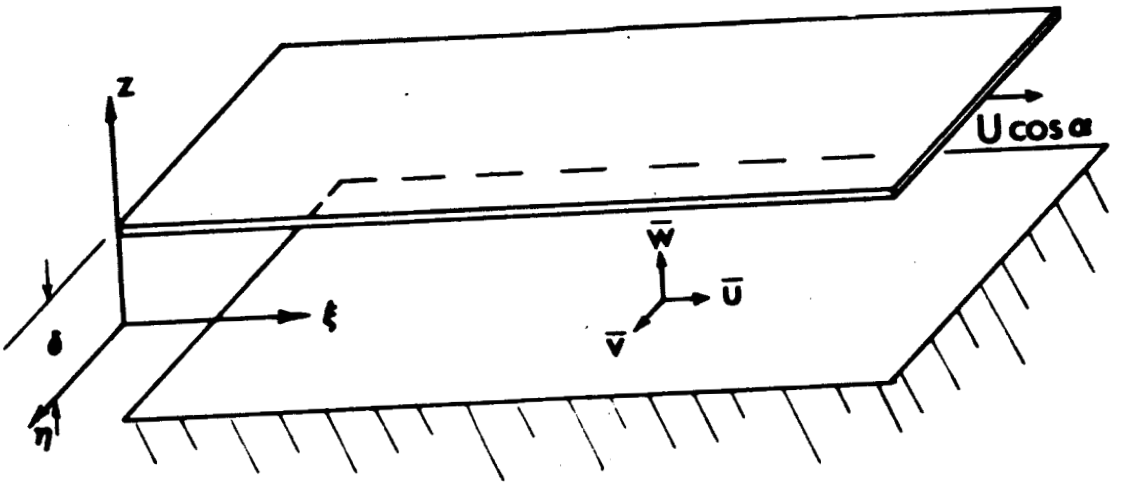

Figure 4. Model for groove and land flow.

the flow will be analyzed as purely Couette and purely Poiseuille and then added vectorially to produce an approximation of the total discharge.

The important physical parameters in this problem are the shearing stress at the wall τ, the density of the fluid ρ, the absolute viscosity of the fluid μ, the time averaged velocity of the fluid, and a characteristic length. Rewriting equations (32) and (33) in a non-dimensional form by incorporating the parameters in Table I, they become:

$$\frac{1}{\delta} \frac{\partial(\rho u_1^2 \bar{\omega}_\xi)}{\partial \xi^*} = \frac{u_1 \mu}{\delta^2} \frac{d^2 U^*}{dz^{*2}} - \frac{\rho u_1^2}{\delta} \frac{d r_\xi}{dz^*}, \tag{34}$$

and

$$\frac{1}{\delta} \frac{\partial(\rho v_1^2 \bar{\omega}_\eta)}{\partial \eta^*} = \frac{v_1 \mu}{\delta^2} \frac{d^2 V^*}{dz^{*2}} - \frac{\rho v_1^2}{\delta} \frac{d r_\eta}{dz^*}. \tag{35}$$

Simplifying,

$$\frac{\partial \bar{\omega}}{\partial \xi^*} - \frac{\mu}{\rho u_1 \delta} \frac{d^2 U^*}{dz^{*2}} + \frac{d r_\xi}{dz^*} = 0, \tag{36}$$

and

$$\frac{\partial \bar{\omega}}{\partial \eta^*} - \frac{\mu}{\rho v_1 \delta} \frac{d^2 V^*}{dz^{*2}} + \frac{d r_\eta}{dz^*} = 0. \tag{37}$$

The boundary conditions for equations (36) and (37) as applied to the visco pump are:

a. Poiseuille flow

$$U_P^* = 0 \qquad \text{at } z^* = \pm 1 \tag{38}$$

$$V_P^* = 0 \qquad \text{at } z^* = \pm 1 \tag{39}$$

Couette flow

$$U_{ct}^* = 0 \qquad \text{at } z^* = -1 \tag{40}$$

$$U_{ct}^* = 1/2 \frac{U \cos \alpha}{u_1} \quad \text{at } z^* = 0 \tag{41}$$

TABLE I

DIMENSIONLESS PARAMETERS

$U^* = \frac{\bar{u}}{u_1}$	Velocity, ξ^* direction
$u_1 = \left[\frac{\tau_{o\xi}}{\rho}\right]^{1/2}$	Reference velocity, ξ^* direction
$V^* = \frac{\bar{v}}{v_1}$	Velocity, η^* direction
$v_1 = \left[\frac{\tau_{o\eta}}{\rho}\right]^{1/2}$	Reference velocity, η^* direction
$r_\xi = \frac{\overline{u'w'}}{u_1^2}$	
$r_\eta = \frac{\overline{v'w'}}{v_1^2}$	
$\bar{\omega}_\xi = \frac{\bar{P} - \bar{P}_1}{\rho u_1^2}$	
$\bar{\omega}_\eta = \frac{\bar{P} - \bar{P}_1}{\rho v_1^2}$	
$R_{1\xi} = \frac{u_1 \delta \rho}{\mu}$	
$R_{1\eta} = \frac{v_1 \delta \rho}{\mu}$	
$\xi^* = \frac{\xi}{\delta}$	
$\eta^* = \frac{\eta}{\delta}$	
$z^* = \frac{z}{\delta}$	

$$V^*_{ct} = 0 \qquad \text{at } z^* = -1 \tag{42}$$

$$V^*_{ct} = -1/2 \frac{U \sin\alpha}{v_1} \text{ at } z^* = 0 \tag{43}$$

b. $$r_\xi = 0 \qquad \text{at } z^* = \pm 1 \tag{44}$$

$$r_\eta = 0 \qquad \text{at } z^* = \pm 1 \tag{45}$$

c. $$\bar{\omega}_\xi = 0 \qquad \text{at } z^* = -1, \quad \xi^* = 0, \quad \eta^* = 0 \tag{46}$$

$$\bar{\omega}_\eta = 0 \qquad \text{at } z^* = -1, \quad \xi^* = 0, \quad \eta^* = 0 . \tag{47}$$

Employing the dimensionless parameters in Table I, the shear at the walls for Poiseuille and Couette flow are related as follows:

a. Poiseuille flow

$$R_{1\xi} = \pm \frac{d U^*_P}{dz^*} \quad \text{at } z^* = \mp 1 \tag{48}$$

$$R_{1\eta} = \pm \frac{dV^*_P}{dz^*} \quad \text{at } z^* = \mp 1 \tag{49}$$

b. Couette flow

$$R_{1\xi} = \frac{d U^*_{ct}}{dz^*} \quad \text{at } z^* = \pm 1 \tag{50}$$

$$R_{1\eta} = \frac{- d V^*_{ct}}{dz^*} \quad \text{at } z^* = \pm 1. \tag{51}$$

Integration of equations (36) and (37) with respect to z^* gives:

$$-\frac{1}{R_{1\xi}} \frac{d U^*}{dz^*} + r_\xi - C_5 z^* = C_6 , \tag{52}$$

and

$$-\frac{1}{R_{1\eta}} \frac{d V^*}{dz^*} + r_\eta - C_7 z^* = C_8 , \tag{53}$$

where the pressure gradients in the ξ^* and η^* directions were assumed

to be constant.

Applying the boundary conditions for Poiseuille flow in the positive ξ direction, equations (52) and (53) become:

$$-\frac{1}{R_{1\xi}} \frac{dU_P^*}{dz^*} + r_\xi - z^* = 0, \tag{54}$$

and

$$-\frac{1}{R_{1\eta}} \frac{dV_P^*}{dz^*} + r_\eta - z^* = 0. \tag{55}$$

Again integrating with respect to z^*, equations (54) and (55) become:

$$U_P^* = \frac{R_{1\xi}}{2}(1 - z^{*2}) + R_{1\xi} \int_{-1}^{z^*} r_{1\xi}\, dz^*, \tag{56}$$

and

$$V_P^* = \frac{R_{1\eta}}{2}(1 - z^{*2}) + R_{1\eta} \int_{-1}^{z^*} r_{1\eta}\, dz^*. \tag{57}$$

Since equations (56) and (57) cannot be solved directly because of the lack of a functional relationship between r_1 and z^*, an expression for U_P^* and V_P^*, in terms of a power series of z^*, is assumed. The velocity distribution in Poiseuille flow is symmetrical about the center line. Therefore, an even power series solution will be used. Hence,

$$U_P^* = C_9 (1 + C_{10} z^{*2} + C_{11} z^{*2N}), \tag{58}$$

and

$$V_P^* = C_{12} (1 + C_{13} z^{*2} + C_{14} z^{*2N'}), \tag{59}$$

where higher order terms are neglected and N and N' are any positive integer greater than one.

Using the boundary conditions expressed in equations (38), (39), (48), and (49), and $U_P^* = \bar{u}_\ell / u_1$ at $z^* = 0$ and $V_P^* = \bar{v}_\ell / v_1$ at $z^* = 0$, equations (58) and (59) become:

$$U_P^* = \frac{\bar{u}_\ell}{u_1} \left(1 + \frac{F_\xi - N}{N - 1} z^{*2} + \frac{1 - F_\xi}{N - 1} z^{*2N}\right) , \tag{60}$$

and

$$V_P^* = \frac{\bar{v}_\ell}{v_1} \left(1 + \frac{F_\eta - N'}{N' - 1} z^{*2} + \frac{1 - F_\eta}{N' - 1} z^{*2N'}\right) . \tag{61}$$

In equations (60) and (61),

$$F_\xi = \frac{u_1 R_{1\xi}}{2\bar{u}_\ell}$$

and

$$F_\eta = \frac{v_1 R_{1\eta}}{2\bar{v}_\ell} ,$$

which when simplified become

$$F_\xi = \frac{\tau_{o\xi}}{\frac{2\mu \bar{u}_\ell}{\delta}}$$

and

$$F_\eta = \frac{\tau_{o\eta}}{\frac{2\mu \bar{v}_\ell}{\delta}} .$$

Therefore, F_ξ and F_η can be expressed as the ratio of the shearing stress on the wall in turbulent flow to the shearing stress on the wall for laminar flow with the same maximum velocity.

Thus,

$$F_\xi = \left(\frac{\tau_o}{\tau_\ell}\right)_\xi = \left(\frac{f_o}{f_\ell}\right)_\xi \tag{62}$$

and

$$F_\eta = \left(\frac{\tau_o}{\tau_\ell}\right)_\eta = \left(\frac{f_o}{f_\ell}\right)_\eta . \tag{63}$$

With the relationship

$$\frac{\partial \bar{P}}{\partial \xi} = \frac{\tau_{o\xi}}{z} \equiv \frac{\mu}{z} \left(\frac{d\bar{u}}{dz}\right)\Bigg|_{z=\delta} ,$$

$\bar{u}_\ell$ is found in terms of the pressure gradient $\partial \bar{P}/\partial \xi$. Hence,

$$\bar{u}_\ell = \frac{\delta^2}{2\mu} \frac{\partial \bar{P}}{\partial \xi} \left[\frac{N-1}{F_\xi - NF_\xi}\right], \tag{64}$$

and similarly,

$$\bar{v}_\ell = \frac{\delta^2}{2\mu} \frac{\partial \bar{P}}{\partial \eta} \left[\frac{N'-1}{F_\eta - N'F_\eta}\right] . \tag{65}$$

Thus equations (60) and (61) become:

$$U_P^* = \frac{\delta^2 K_{1\xi}}{\mu u_1} \frac{\partial \bar{P}}{\partial \xi} \left(1 + \frac{F_\xi - N}{N-1} z^{*2} + \frac{1-F_\xi}{N-1} z^{*2N}\right) , \tag{66}$$

and

$$V_P^* = \frac{\delta^2 K_{1\eta}}{\mu v_1} \frac{\partial \bar{P}}{\partial \eta} \left(1 + \frac{F_\eta - N'}{N'-1} z^{*2} + \frac{1-F_\eta}{N'-1} z^{*2N'}\right) , \tag{67}$$

where

$$K_{1\xi} = \frac{1}{2} \left(\frac{N-1}{F_\xi - NF_\xi}\right) ,$$

and

$$K_{1\eta} = \frac{1}{2} \left(\frac{N'-1}{F_\eta - N'F_\eta}\right) .$$

Equations (66) and (67) are the non-dimensional velocity equations for Poiseuille flow in the visco pump.

Applying the boundary conditions for Couette flow to equations (52) and (53) and integrating, the describing equations for the velocity become:

$$U^*_{ct} = R_{1\xi} \quad (Z^* + 1) + R_{1\xi} \int_{-1}^{z^*} r_\xi \quad dz^* \quad , \tag{68}$$

and

$$V^*_{ct} = - R_{1\eta} \quad (Z^* + 1) + R_{1\eta} \int_{-1}^{z^*} r_\eta \quad dz^* \quad . \tag{69}$$

Because of the inability in evaluating the integral in equations (68) and (69), a power series solution will again be assumed. However, in Couette flow the velocity distribution is not symmetrical about the center line, so an odd power series is used. Therefore,

$$U^*_{ct} = C_{15} \left(1 + C_{16}\, z^* + C_{17}\, z^{*\,2M+1}\right) \quad , \tag{70}$$

and

$$V^*_{ct} = C_{18} \left(1 + C_{19}\, z^* + C_{20}\, z^{*\,2M'+1}\right) \quad , \tag{71}$$

where higher order terms are neglected and M and M' are any positive integer. Using the boundary conditions as expressed in equations (40), (41), (42), (43), (50), and (51), equations (70) and (71) become:

$$U^*_{ct} = \frac{U \cos \alpha}{2\, u_1} \left(1 + \frac{2\,M - H_\xi \quad + 1}{2M}\, z^* + \frac{H_\xi \quad - 1}{2\,M}\, z^{*2M+1}\right) , \tag{72}$$

and

$$V^*_{ct} = - \frac{U \sin \alpha}{2\, v_1} \left(1 + \frac{2M' - H_\eta \quad + 1}{2M'}\, z^* + \frac{H_\eta \quad -1}{2M'} z^{*2M'+1}\right) , \tag{73}$$

where

$$H_\xi \quad = \frac{2R_{1\xi}\ u_1}{U \cos \alpha} \quad ,$$

and

$$H_\eta \quad = \frac{2R_{1\eta}\ v_1}{U \sin \alpha} \quad .$$

Equations (72) and (73) are the non-dimensional velocity equations for Couette flow in the ξ^* and η^* directions.

The velocity distribution in the visco pump is represented by the vectorial summation of the Couette and Poiseuille velocity components. Thus,

$$U^* = U^*_{ct} - U^*_P$$

and

$$V^* = V^*_{ct} - V^*_P \ ,$$

or

$$U^* = \frac{U \cos\alpha}{2\, u_1}\left[1 + \frac{1 + 2M - H_\xi}{2M}\, z^* + \frac{H_\xi - 1}{2M}\, z^{*2M+1}\right]$$

$$- \frac{\delta^2 K_{1\xi}}{\mu u_1} \frac{\partial \bar{P}}{\partial \xi}\left[1 + \frac{F_\xi - N}{N-1} z^{*2} + \frac{1 - F_\xi}{N-1}\, z^{*2N}\right] , \qquad (74)$$

and

$$V^* = -\frac{U \sin\alpha}{2\, v_1}\left[1 + \frac{1 + 2M' - H_\eta}{2M'}\, z^* + \frac{H_\eta - 1}{2M'}\, z^{*2M'+1}\right]$$

$$- \frac{\delta^2 K_1}{\mu v_1} \frac{\partial \bar{P}}{\partial \eta}\left[1 + \frac{F_\eta - N'}{N'-1} z^{*2} + \frac{1 - F_\eta}{N'-1}\, z^{*2N'}\right] . \qquad (75)$$

From experimental measurements of Poiseuille flow between parallel flat plates performed by Laufer [12], Pai determined a relation between N and F_ξ and N' and F_η. Thus,

$$\left.\begin{aligned} N &= 1.40\, F_\xi \\ \text{and} \\ N' &= 1.40\, F_\eta \end{aligned}\right\} . \qquad (76)$$

As a similar relation between M and H_ξ and M' and H_η has not been experimentally determined, the same relationship that exists in Poiseuille flow will be assumed. Hence,

$$\left.\begin{aligned} M &= 1.40\, H_\xi \\ \text{and} \qquad M' &= 1.40\, H_\eta \end{aligned}\right\} \qquad (77)$$

Simplifying, equations (74) and (75) become:

$$U^* = \frac{U\cos\alpha}{2\,u_1}\left[1 + \frac{1 + 1.8\,H_\xi}{2.8\,H_\xi}\,z^* + \frac{H_\xi - 1}{2.8\,H_\xi}\,z^{*2M+1}\right]$$

$$- \frac{\delta^2 K_{1\xi}}{\mu u_1}\,\frac{\partial \bar{P}}{\partial \xi}\left[1 + \frac{-.4\,F_\xi}{1.4\,F_\xi - 1}\,z^{*2} + \frac{1 - F}{1.4\,F_\xi - 1}\,z^{*2N}\right], \qquad (78)$$

and

$$V^* = -\frac{U\sin\alpha}{2\,v_1}\left[1 + \frac{1 + 1.8\,H_\eta}{2.8\,H_\eta}\,z^* + \frac{H_\eta - 1}{2.8\,H_\eta}\,z^{*2M'+1}\right]$$

$$- \frac{\delta^2 K_{1\eta}}{\mu v_1}\,\frac{\partial \bar{P}}{\partial \eta}\left[1 + \frac{-.4\,F_\eta}{1.4\,F_\eta - 1}\,z^{*2} + \frac{1 - F_\eta}{1.4\,F_\eta - 1}\,z^{*2N'}\right]. \qquad (79)$$

Equations (78) and (79) apply to both the lands and the grooves. Therefore, the mean velocity components are as follows:

along the lands,

$$\bar{u}_r = \frac{U\cos\alpha}{2}\left[1 + \frac{1 + 1.8\,H_\xi}{2.8\,H_\xi}\left(\frac{2z}{c}\right) + \frac{H_\xi - 1}{2.8\,H_\xi}\left(\frac{2z}{c}\right)^{2M+1}\right]$$

$$- \frac{c^2 K_{1\xi}}{4\mu}\left(\frac{\partial \bar{P}}{\partial \xi}\right)_r\left[1 + \frac{-.4\,F_\xi}{1.4\,F_\xi - 1}\left(\frac{2z}{c}\right)^2 + \frac{1 - F_\xi}{1.4\,F_\xi - 1}\left(\frac{2z}{c}\right)^{2N}\right]; \qquad (80)$$

along the grooves,

$$\bar{u}_g = \frac{U \cos\alpha}{2}\left[1 + \frac{1 + 1.8\,H_\xi}{2.8\,H_\xi}\left(\frac{2z}{h_g}\right) + \frac{H_\xi - 1}{2.8\,H_\xi}\left(\frac{2z}{h_g}\right)^{2M+1}\right]$$

$$- \frac{h_g^2\,K_{1\xi}}{4\mu}\left(\frac{\partial \bar{P}}{\partial \xi}\right)_g\left[1 + \frac{-.4\,F_\xi}{1.4\,F_\xi - 1}\left(\frac{2z}{h_g}\right)^2 + \frac{1 - F_\xi}{1.4\,F_\xi - 1}\right.$$

$$\left.\left(\frac{2z}{h_g}\right)^{2N}\right]; \tag{81}$$

across the lands,

$$\bar{v} = -\frac{U \sin\alpha}{2}\left[1 + \frac{1 + 1.8\,H_\eta}{2.8\,H_\eta}\left(\frac{2z}{c}\right) + \frac{H_\eta - 1}{2.8\,H_\eta}\left(\frac{2z}{c}\right)^{2M'+1}\right]$$

$$- \frac{c^2\,K_{1\eta}}{4\mu}\left(\frac{\partial \bar{P}}{\partial \eta}\right)_r\left[1 + \frac{-.4\,F_\eta}{1.4\,F_\eta - 1}\left(\frac{2z}{c}\right)^2 + \frac{1 - F_\eta}{1.4\,F_\eta - 1}\left(\frac{2z}{c}\right)^{2N'}\right];$$

and across the grooves,

$$\bar{v}_g = -\frac{U \sin\alpha}{2}\left[1 + \frac{1 + 1.8\,H_\eta}{2.8\,H_\eta}\left(\frac{2z}{h_g}\right) + \frac{H_\eta - 1}{2.8\,H_\eta}\left(\frac{2z}{h_g}\right)^{2M'+1}\right]$$

$$- \frac{h_g^2\,K_{1\eta}}{4\mu}\left(\frac{\partial \bar{P}}{\partial \eta}\right)_g\left[1 + \frac{-.4\,F_\eta}{1.4\,F_\eta - 1}\left(\frac{2z}{h_g}\right)^2 + \frac{1 - F_\eta}{1.4\,F_\eta - 1}\left(\frac{2z}{h_g}\right)^{2N'}\right]. \tag{83}$$

The total flow in the visco pump is composed of three basic components: ξ directed land flow, ξ directed groove flow, and η directed groove or land flow. The axial velocity components may be expressed as:

$$\bar{u}_y = \bar{u} \sin\alpha \tag{84}$$

and

$$\bar{v}_y = \bar{v} \cos\alpha\,. \tag{85}$$

From these velocity components, the flow components $Q_{\xi r}$, $Q_{\xi g}$, and $Q_{\eta r}$ or $Q_{\eta g}$, are computed. For the visco pump the width of the flow path for the ξ land flow is $(1 - \gamma)\,\pi D$ and the path width for ξ groove flow is $\gamma \pi D$. The axial component of the ξ land flow becomes:

$$Q_{\xi r} = (1 - \gamma)\,\pi D \int_{-c/2}^{c/2} \bar{u}_r \sin\alpha \, dz$$

or

$$Q_{\xi r} = (1 - \gamma)\,\pi D \left\{ \frac{U c \cos\alpha \sin\alpha}{2} \right.$$

$$- \frac{c^2 K_{1\xi} \sin\alpha}{4\mu} \left(\frac{\partial \bar{P}}{\partial \xi}\right)_r \left[c + \frac{c}{3} \left(\frac{-.4\, F_\xi}{1.4\, F_\xi - 1} \right) + \frac{c}{2N + 1} \right.$$

$$\left. \left. \left(\frac{1 - F_\xi}{1.4\, F_\xi - 1} \right) \right] \right\} \quad . \tag{86}$$

Similarly,

$$Q_{\xi g} = \gamma \pi D \left\{ \frac{U h_g \cos\alpha \sin\alpha}{2} \right.$$

$$- \frac{h_g^2 K_{1\xi} \sin\alpha}{4\mu} \left(\frac{\partial \bar{P}}{\partial \xi}\right)_g \left[h_g + \frac{h_g}{3} \left(\frac{-.4\, F_\xi}{1.4\, F_\xi - 1} \right) + \frac{h_g}{2N + 1} \right.$$

$$\left. \left. \left(\frac{1 - F_\xi}{1.4\, F_\xi - 1} \right) \right] \right\} \quad , \tag{87}$$

$$Q_{\eta r} = \pi D \left\{ - \frac{\bar{U} c \sin\alpha \cos\alpha}{2} \right.$$

$$- \frac{c^2 K_{1\eta} \cos\alpha}{4\mu} \left(\frac{\partial \bar{P}}{\partial \eta}\right)_r \left[c + \frac{c}{3} \left(\frac{-.4\, F_\eta}{1.4\, F_\eta - 1} \right) + \frac{c}{2N' + 1} \right.$$

$$\left. \left. \left(\frac{1 - F_\eta}{1.4\, F_\eta - 1} \right) \right] \right\} \quad , \tag{88}$$

and

$$Q_{\eta g} = \pi D \left\{ - \frac{U\, h_g \sin\alpha \cos\alpha}{2} \right.$$

$$\left. - \frac{h_g^2 K_{1\eta} \cos\alpha}{4\mu} \left(\frac{\partial \bar{P}}{\partial \eta}\right)_g \left[h_g + \frac{h_g}{3} \left(\frac{-.4\, F_\eta}{1.4\, F_\eta - 1} \right) + \frac{h_g}{2N' + 1} \right.\right.$$

$$\left.\left. \left(\frac{1 - F_\eta}{1.4\, F_\eta - 1} \right) \right] \right\} . \tag{89}$$

The pressure gradients in equations (86) through (89) can be re-written in terms of the axial pressure gradient. Thus,

$$\frac{\partial \bar{P}}{\partial \xi} = \frac{d\bar{P}}{dy} \sin\alpha , \tag{90}$$

and

$$(1 - \gamma) \left(\frac{\partial \bar{P}}{\partial \eta}\right)_r + \left(\frac{\partial \bar{P}}{\partial \eta}\right)_g = \frac{d\bar{P}}{dy} \cos\alpha . \tag{91}$$

Substituting equation (90) into equations (86) and (87) and simplifying using the terms in Table II, the flow components become:

$$Q_{\xi r} = (1 - \gamma)\, \pi D \left\{ \frac{U\, c \cos\alpha \sin\alpha}{2} \right.$$

$$\left. - \frac{c^3 K_{1\xi} \sin^2\alpha}{4\mu} \frac{d\bar{P}}{dy} \left[1 - K_{2\xi} + K_{3\xi} \right] \right\} , \tag{92}$$

and

$$Q_{\xi g} = \gamma \pi D \left\{ \frac{U \beta\, c \cos\alpha \sin\alpha}{2} \right.$$

$$\left. - \frac{(\beta c)^3 K_{1\xi} \sin^2\alpha}{4\mu} \frac{d\bar{P}}{dy} \left[1 - K_{2\xi} + K_{3\xi} \right] \right\} . \tag{93}$$

The total flow from the visco pump is:

$$Q = Q_{\xi g} + Q_{\xi r} + Q_{\eta r} = Q_{\xi g} + Q_{\xi r} + Q_{\eta g} ,$$

since

$$Q_{\eta g} = Q_{\eta r} .$$

TABLE II

DIMENSIONLESS SIMPLIFYING TERMS

$$K_{1\xi} = \frac{1}{2}\left(\frac{N-1}{F_\xi - NF_\xi}\right) = \frac{1}{2}\left(\frac{1.4\,F_\xi - 1}{F_\xi - 1.4\,F_\xi^2}\right)$$

$$K_{1\eta} = \frac{1}{2}\left(\frac{N'-1}{F_\eta - N'F_\eta}\right) = \frac{1}{2}\left(\frac{1.4\,F_\eta - 1}{F_\eta - 1.4\,F_\eta^2}\right)$$

$$K_{2\xi} = \frac{0.4\,F_\xi}{4.2\,F_\xi - 3}$$

$$K_{2\eta} = \frac{0.4\,F_\eta}{4.2\,F_\eta - 3}$$

$$K_{3\xi} = \frac{1 - F_\xi}{3.92\,F_\xi^2 - 1.4\,F_\xi - 1}$$

$$K_{3\eta} = \frac{1 - F_\eta}{3.92\,F_\eta^2 - 1.4\,F_\eta - 1}$$

$$K_4 = -3\,K_{1\xi}\,(1 - K_{2\xi} + K_{3\xi})$$

$$K_5 = -3\,K_{1\eta}\,(1 - K_{2\eta} + K_{3\eta})$$

$$I_1 = (1 - \gamma)\,t^2$$

$$I_2 = \beta^3 \gamma\, t^2$$

$$I_3 = \frac{\beta^3}{\gamma + \beta^3 (1 - \gamma)}$$

$$I_4 = t\left[1 - \gamma + \gamma\beta - \frac{\gamma + \beta^3 (1 - \gamma) + \gamma(\beta - 1)}{\gamma + \beta^3 (1 - \gamma)}\right]$$

Solving for $\left(\partial \bar{P}/\partial \eta \right)_r$ from equation (91) and simplifying:

$$\left(\frac{\partial \bar{P}}{\partial \eta}\right)_r = \frac{\beta^3 \frac{d\bar{P}}{dy} \cos\alpha}{\gamma + \beta^3 (1-\gamma)} +$$

$$\frac{4\mu U \sin\alpha (\beta - 1)\gamma}{2c^2 K_{1\eta} (1 - K_{2\eta} + K_{3\eta}) \left[\gamma + \beta^3 (1-\gamma)\right]} .$$

Therefore, $Q_{\eta r}$ becomes:

$$Q_{\eta r} = \pi D \left\{ - \frac{U c \sin\alpha \cos\alpha}{2} - \frac{(c\beta)^3 K_{1\eta} \cos^2\alpha}{4\mu \left[\gamma + \beta^3 (1-\gamma)\right]} \frac{d\bar{P}}{dy} \right.$$

$$\left. (1 - K_{2\eta} + K_{3\eta}) - \frac{c U \sin\alpha \cos\alpha (\beta - 1)}{2 \left[\gamma + \beta^3 (1-\gamma)\right]} \right\} . \qquad (95)$$

Writing the sine and cosine functions as tangents, the equation for the total discharge from the visco pump is:

$$Q = (1-\gamma)\pi D \left[\frac{U c t}{2} - \frac{c^3 K_{1\xi} t^2}{4\mu} (1 - K_{2\xi} + K_{3\xi}) \frac{d\bar{P}}{dy} \right]$$

$$+ \gamma \pi D \left[\frac{U \beta c t}{2} - \frac{(\beta c)^3 K_{1\xi} t^2}{4\mu} (1 - K_{2\xi} + K_{3\xi}) \frac{d\bar{P}}{dy} \right]$$

$$+ \pi D \left[- \frac{U c t}{2} - \frac{(\beta c)^3 K_{1\eta}}{4\mu \left[\gamma + \beta^3 (1-\gamma)\right]} (1 - K_{2\eta} + K_{3\eta}) \frac{d\bar{P}}{dy} \right.$$

$$\left. - \frac{c U t \gamma (\beta - 1)}{2 \left[\gamma + \beta^3 (1-\gamma)\right]} \right] . \qquad (96)$$

In equation (96) the only terms to be determined empirically are functions of F_ξ and F_η which are related to Poiseuille flow. Hence, the assumption involved in equation (77) is of no consequence in this solution. Applying equation (96) to a visco seal, simplifying with the terms in Table II, and substituting

$$-\frac{\Delta P}{L} = \frac{d\bar{P}}{dy} ,$$

the sealing coefficient is formed. Thus,

$$\Lambda \equiv \frac{6\,\mu\,U\,L}{c^2\,\Delta P} = K_4 \left(\frac{I_1 + I_2}{I_4}\right) + K_5 \left(\frac{I_3}{I_4}\right). \tag{97}$$

In equation (97) when K_4 and K_5 are unity, the equation reduces to the laminar form of the sealing coefficient as in equation (18). The terms K_4 and K_5 in equation (97) can be evaluated by two methods. K_4 and K_5 could be determined by observing actual test data from the visco seal. The solution that will be incorporated in this work will be to estimate K_4 and K_5 from experimental data for common pipe flow. This procedure will allow K_4 and K_5, and thus equation (97), to be predicted before any experimental data on the visco seal are obtained.

Pinkus [13] predicted that for rotating concentric cylinders, turbulence would be initiated at or before a Reynolds number equal to:

$$Re \leq 41.1 \left[\frac{D}{2c}\right]^{1/2} . \tag{98}$$

For the visco seal an average critical Reynolds number is defined as:

$$Re_{crit.} = 41.1 \left[\frac{D/2}{(1-\gamma)\,c + \gamma\beta\,c}\right]^{1/2} . \tag{99}$$

In Figure 5, which relates resistance coefficients and Reynolds numbers for pipe flow, the resistance coefficient for laminar flow is represented by the equation:

$$f_l = \frac{64}{Re_{\bar{p}}} . \tag{100}$$

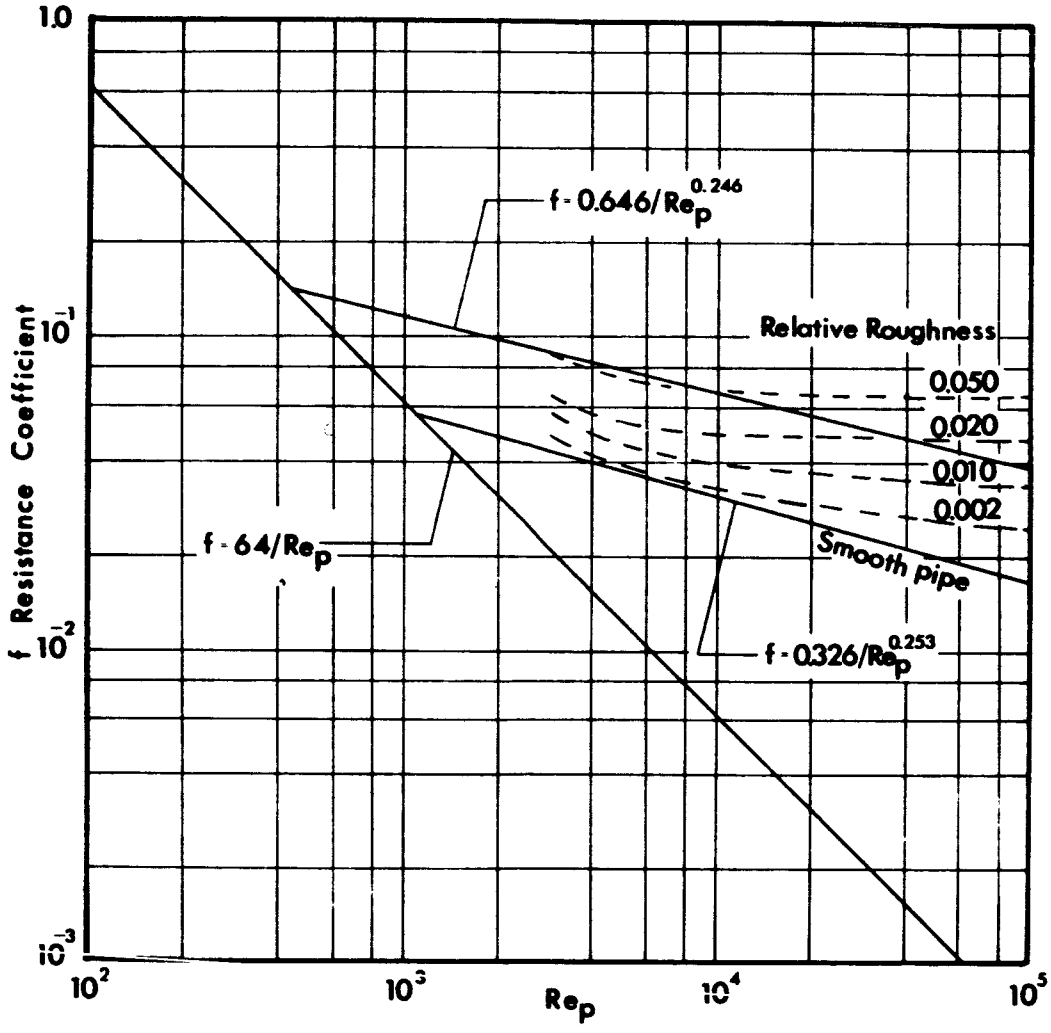

Figure 5. Resistance coefficient versus Reynolds number for pipe flow.

The coefficient of resistance in the transition and turbulent regions was represented by two lines. One line was estimated by extending a straight line from the turbulent smooth pipe curve to its interception with equation (100). This line is represented by the equation,

$$f_{o\xi} = \frac{0.326}{Re_p^{0.253}}, \tag{101}$$

corresponding to flow along the grooves. The other line representing the flow across the grooves was assumed to be typified by a line constructed by extending the turbulent curve for a roughness ratio of approximately 0.03 to intercept with equation (100). This line represented by the equation,

$$f_{o\eta} = \frac{0.646}{Re_p^{0.246}}, \tag{102}$$

corresponds approximately to the flow through corrugated pipe. This procedure, of course, represents the transition zone as a straight line. Assuming the critical pipe Reynolds number occurs at

$$Re_p = 2000,$$

the term F_ξ is evaluated, according to equation (62) for a given Reynolds number in the seal, by computing the ratio of resistance coefficient for turbulent flow, using the lower turbulent line in Figure 5, to the resistance coefficient for laminar flow, both at the pipe Reynolds number of,

$$Re_p = (2000 \cos \alpha) \frac{Re_c}{Re_{crit.}}, \tag{103}$$

where $Re_{crit.}$ is defined by equation (99). The term F_η, equation (63), is evaluated in a similar manner except at a pipe Reynolds number of,

$$Re_p = (2000 \sin \alpha) \frac{Re_c}{Re_{crit.}}, \tag{104}$$

and using the upper turbulent line in Figure 5. The quantities K_4, which is a function of F_ξ, and K_5, which is a function of F_η, can now be determined.

When the operation of the seal is laminar, i.e., F_ξ and F_η are equal to one, K_4 and K_5 are both unity and the sealing coefficient becomes identical to equation (18). As the speed increases, F_ξ increases causing K_4 to decrease and thus the sealing coefficient begins to decrease. At even higher speeds, F_η also begins to increase causing K_5 to decrease, producing a greater decrease in the sealing coefficient. A computer program, compiled for an I.B.M. 7040 computer, to determine the theoretical sealing coefficient is found in Appendix B.

III. GENERALIZING THE THEORETICAL SEALING COEFFICIENT FOR LAMINAR AND TURBULENT OPERATION

In Figures 6 through 9 the theoretical sealing coefficients (hereafter referred to as Λ_T), equation (97), as a function of β for various values of Reynolds number, α, and γ are shown. Several observations may be made regarding these figures:

1. The optimum screw geometry in the laminar range is not the optimum geometry for turbulent operation. As shown in Figure 6, a seal having an α of 5.81° has a minimum sealing coefficient for laminar operation when $\gamma = 0.5$ and $\beta = 6.5$. However, when operation becomes turbulent the minimum value of the sealing coefficient is found at higher values of γ and β. At higher α values the same observation can be made. However, the shift in the optimum β becomes smaller.

2. The β producing the minimum sealing coefficient in the turbulent range increases with increasing Reynolds number. This effect is less significant for large α than for small α.

3. In both laminar and turbulent flow, a given change in β produces a greater change in Λ_T with screws having large α than with small α. Thus, from the standpoint of pressure stability the lower values of α are to be preferred.

4. In laminar operation the optimum γ for any screw is 0.5. However, in turbulent flow the sealing coefficient is improved slightly as γ is increased from 0.5 to 0.7.

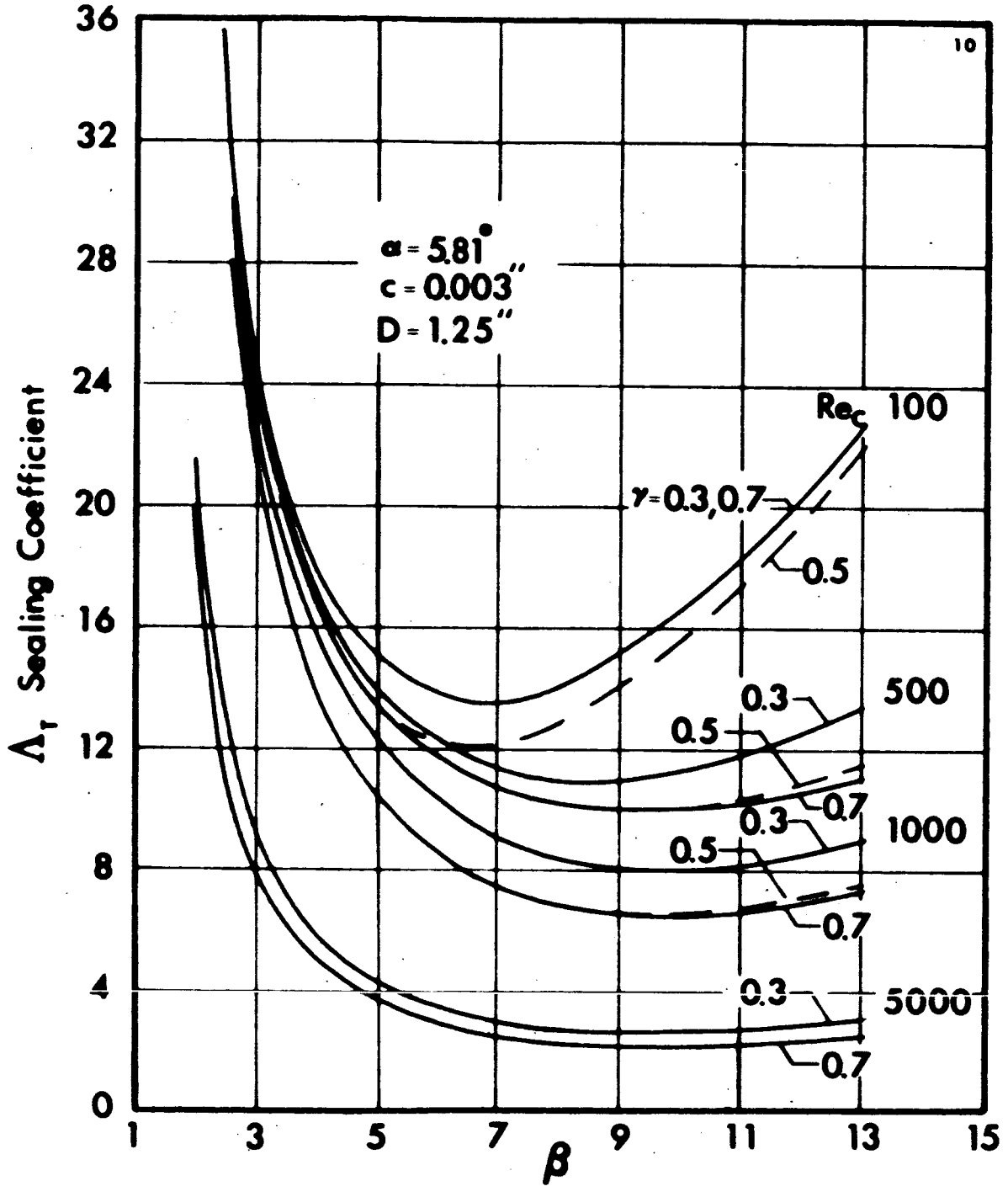

Figure 6. Theoretical sealing coefficient as a function of β, Re_c, and γ for $\alpha = 5.81°$, $c = 0.003$ in., and $D = 1.25$ in.

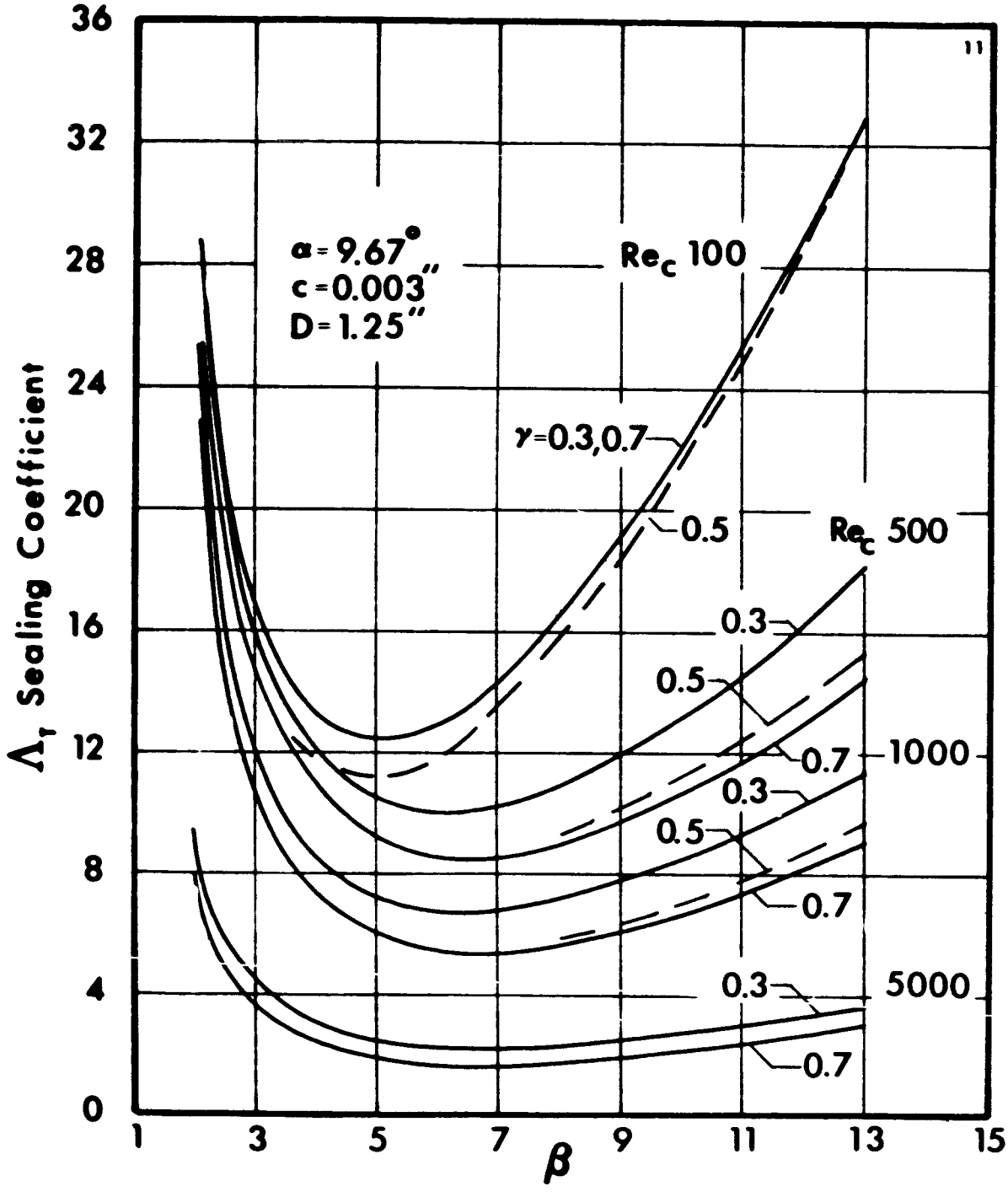

Figure 7. Theoretical sealing coefficient as a function of β, Re_c, and γ for $\alpha = 9.67°$, c = 0.003 in., and D = 1.25 in.

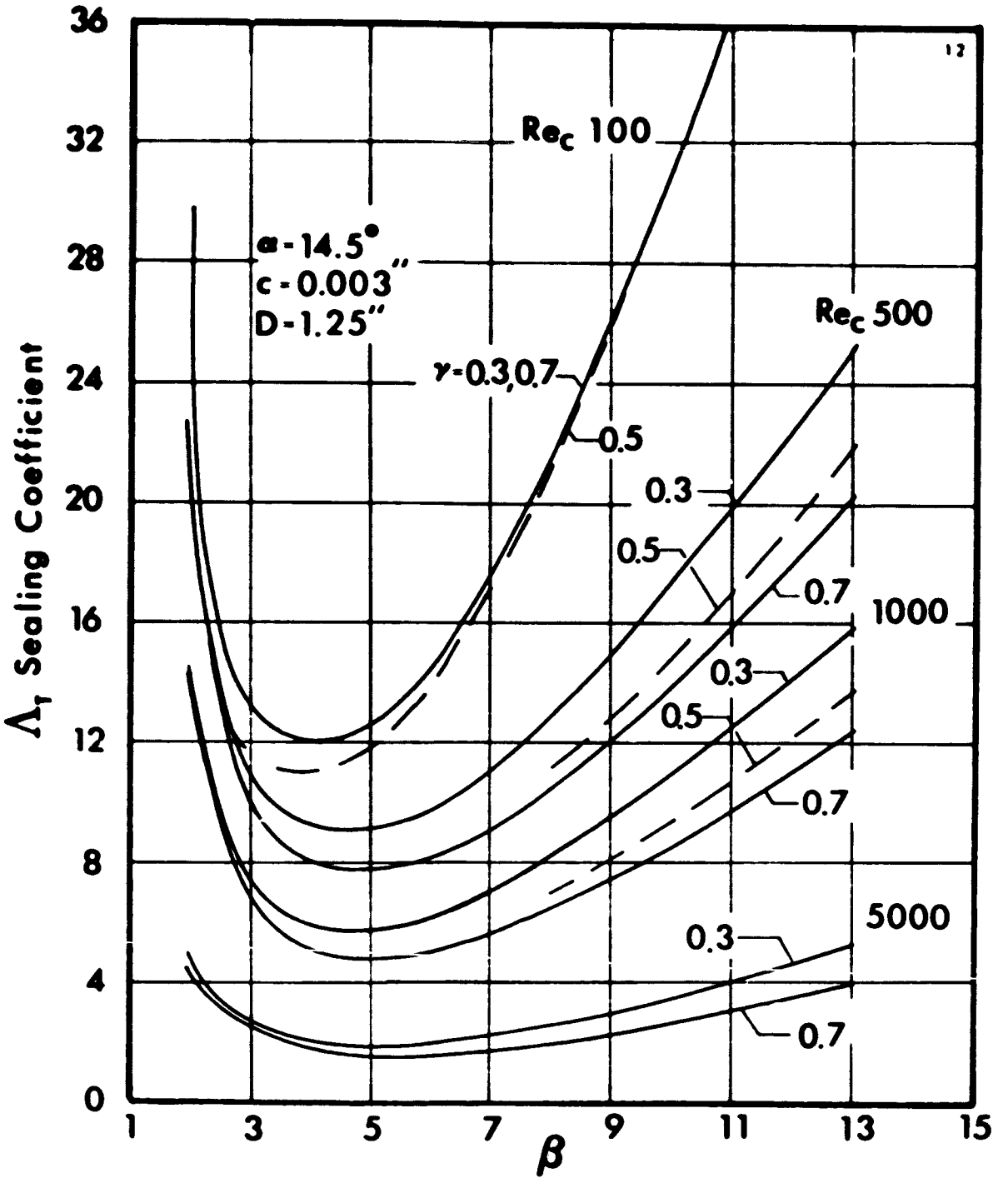

Figure 8. Theoretical sealing coefficient as a function of β, Re_c, and γ for $\alpha = 14.5°$, $c = 0.003$ in., and $D = 1.25$ in.

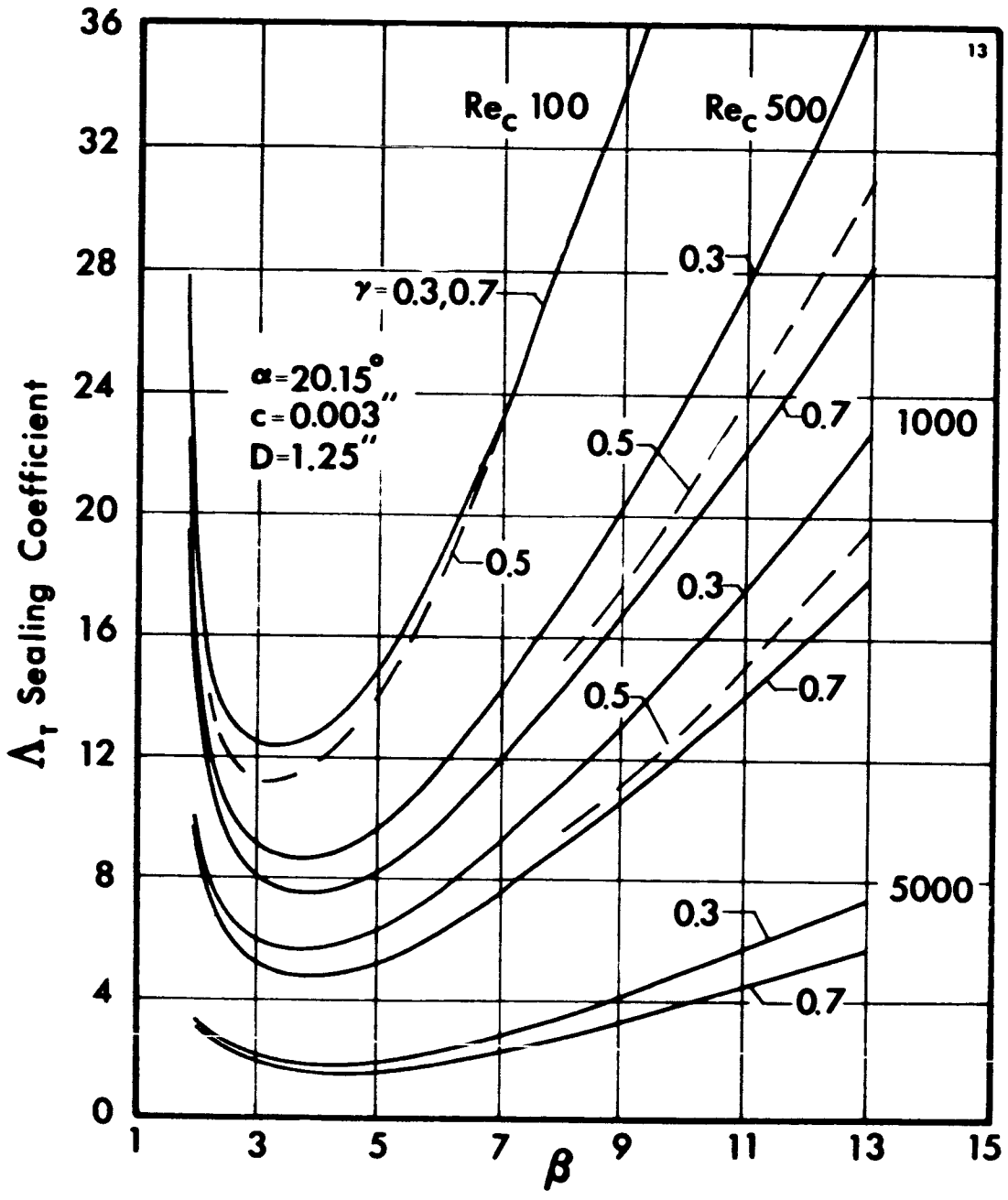

Figure 9. Theoretical sealing coefficient as a function of β, Re_c, and γ for $\alpha = 20.15°$, $c = 0.003$ in., and $D = 1.25$ in.

5. For seals which must operate in both the laminar and turbulent regions, the smaller helix angles will give the best values of the sealing coefficient for both regions.

6. The transition from laminar to turbulent operation is a function of γ. As γ increases the onset of turbulence occurs at lower Reynolds numbers.

7. As the visco seal operation begins to be turbulent the effect of γ on Λ_T at the larger β values is rather pronounced. However, as the degree of turbulence increases this effect becomes less pronounced.

8. At a Reynolds number of 100, Λ_T is the same as the one computed in equation (18), which is independent of Reynolds number.

CHAPTER III

TEST FACILITY AND EXPERIMENT PROCEDURE

I. TEST FACILITIES

The visco seal test section and drive is shown in Figure 10. A detailed description of the design and construction of the experimental facility is presented in Reference [14]. A schematic diagram of the test section is shown in Figure 11. The sealant fluid, which was distilled water in all tests reported, was introduced under regulated pressure through the sealant inlet. Pressure taps and thermocouples are located along the axis of the test sleeve, the dimensional location of which are shown in Figure 12. Inductance probes located in two planes and 90° apart are used to determine the eccentricity between the test sleeve and spindle. A torque arm connected to a strain gage bridge is used to measure the frictional torque. Since the torque measured under some operational conditions is very low, the test sleeve is mounted on eight hydrostatic bearing pads to minimize static friction. The dimensions of the test spindles are presented in Table III. Test spindles 1, 2, 3, 4, 2B, 3B, and 4 B shown in Figure 13, were threaded the total seal length. Spindles 5, 6, and 7, shown in Figure 13, were constructed with end dams in order to study the end effects of the seal and the phenomenon of air ingestion.

II. TEST PROCEDURE

During a test run the data recorded included spindle speed, torque, eccentricity, pressure distribution, and temperature distribution. Using the information in Table III, the recorded experimental data, and the physical properties of the test fluid, the experimental sealing coefficient (hereafter referred to as Λ_E), dissipation function, and the friction parameter were calculated. Lambda, dissipation function, and friction parameter were plotted versus Reynolds number based on the clearance.

The quantity $\Delta P/L$ in equation (97) for Λ_E may be interpreted in two ways. In a practical application this value should be $(P_{supply} - P_{atmosphere})/L$. However, in this study the effect of screw geometry on the sealing coefficient was a factor of major concern. Therefore, in

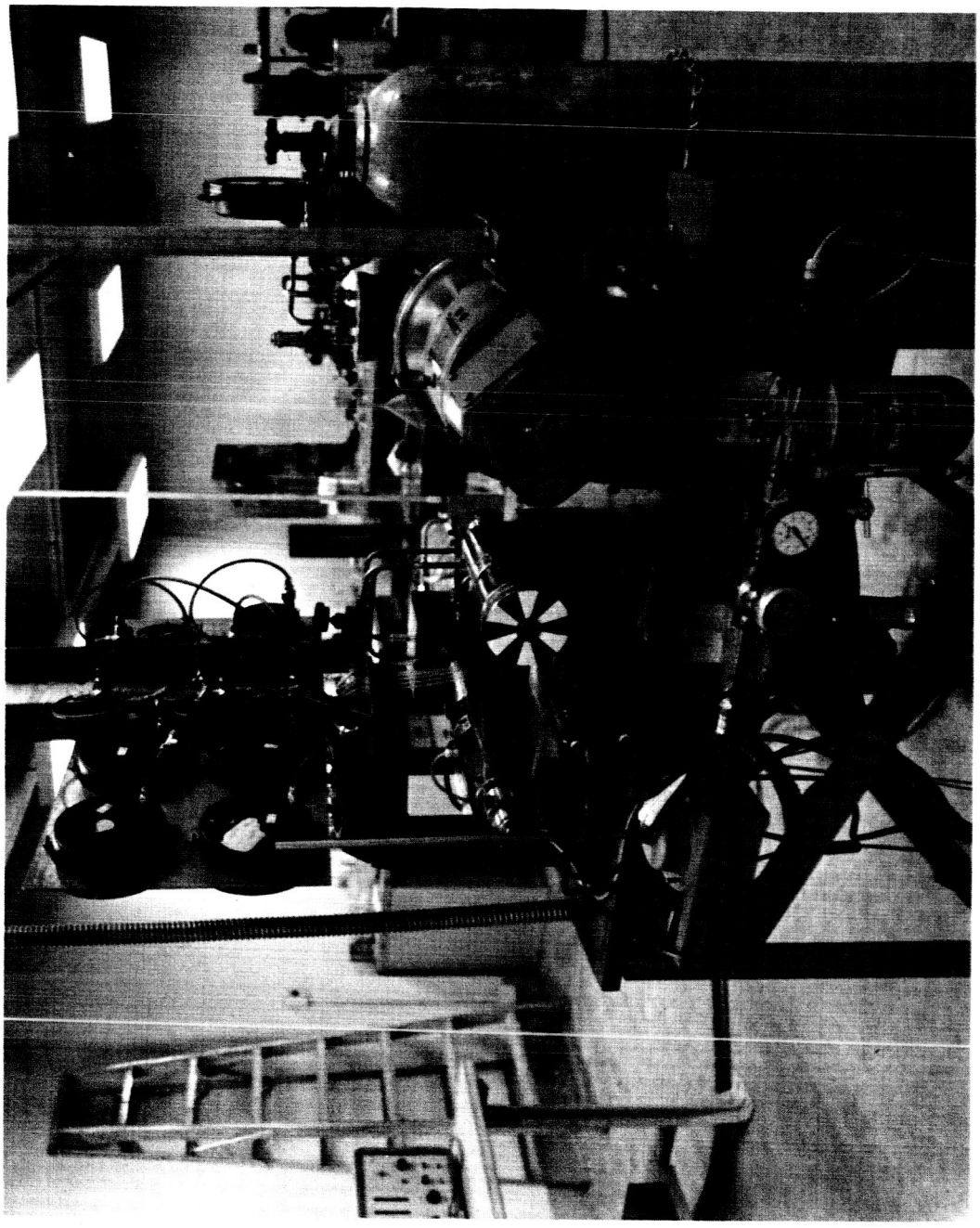

Figure 10. Visco seal test facilities.

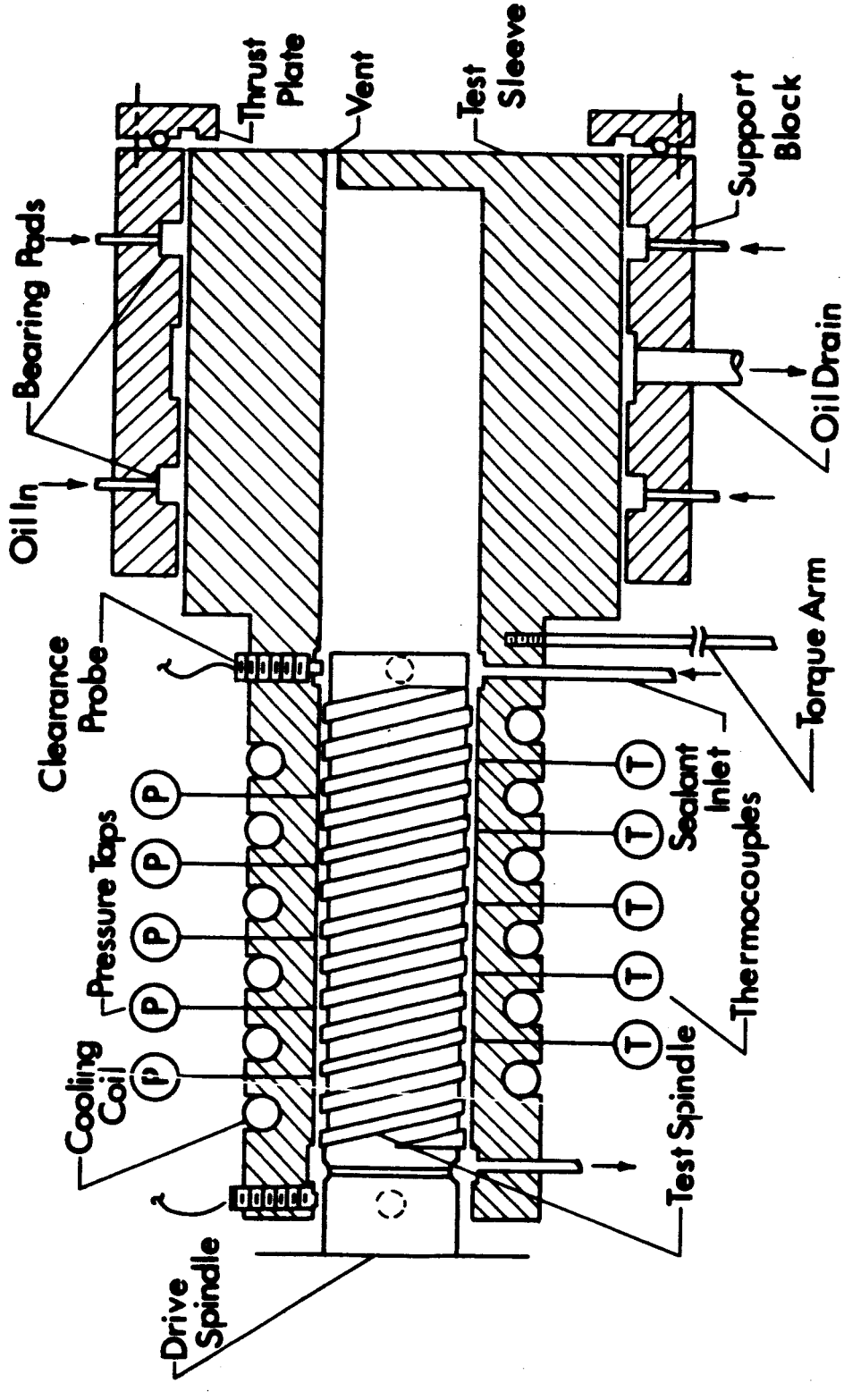

Figure 11. Schematic diagram of the visco seal test section.

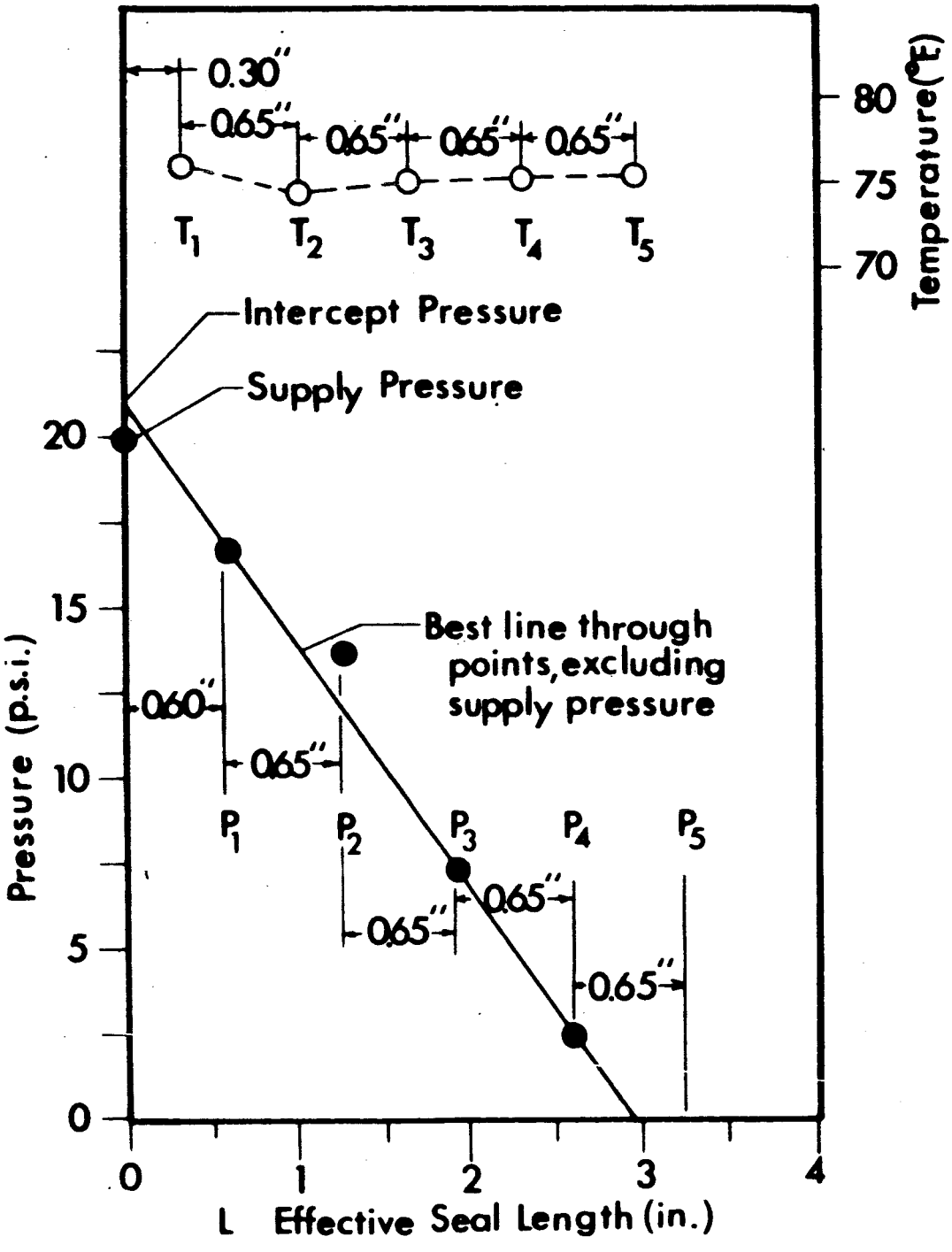

Figure 12. Typical pressure and temperature gradients in the visco seal.

TABLE III

DIMENSIONS AND GEOMETRIC PARAMETERS FOR TEST SEALS

Test Seal No.	D Diameter Inches	c Clearance Inches	h Groove Depth Inches	a Land Width Inches	b Groove Width Inches	α Angle Angle Degrees	β $\frac{(h+c)}{c}$	γ $\frac{b}{(a+b)}$
1	1.2430	0.0042	0.0101	0.0934	0.1596	14.5	3.38	0.631
2	1.2465	0.00235	0.0116	0.1176	0.0494	9.67	5.94	0.296
3	1.2461	0.00265	0.0137	0.0828	0.0842	9.67	6.16	0.504
4	1.2461	0.00265	0.0128	0.0514	0.1156	9.67	5.84	0.692
2B	1.2420	0.0047	0.00925	0.1176	0.0494	9.67	2.96	0.296
3B	1.2408	0.0053	0.01165	0.0828	0.0842	9.67	3.09	0.504
4B	1.2408	0.0053	0.01015	0.0514	0.1156	9.67	2.96	0.692
5	1.2455	0.00295	0.0179	0.1585	0.0607	5.81	6.96	0.277
6	1.2455	0.00295	0.0180	0.1070	0.1083	5.81	7.00	0.502
7	1.2455	0.00295	0.0180	0.0609	0.1600	5.81	7.00	0.724

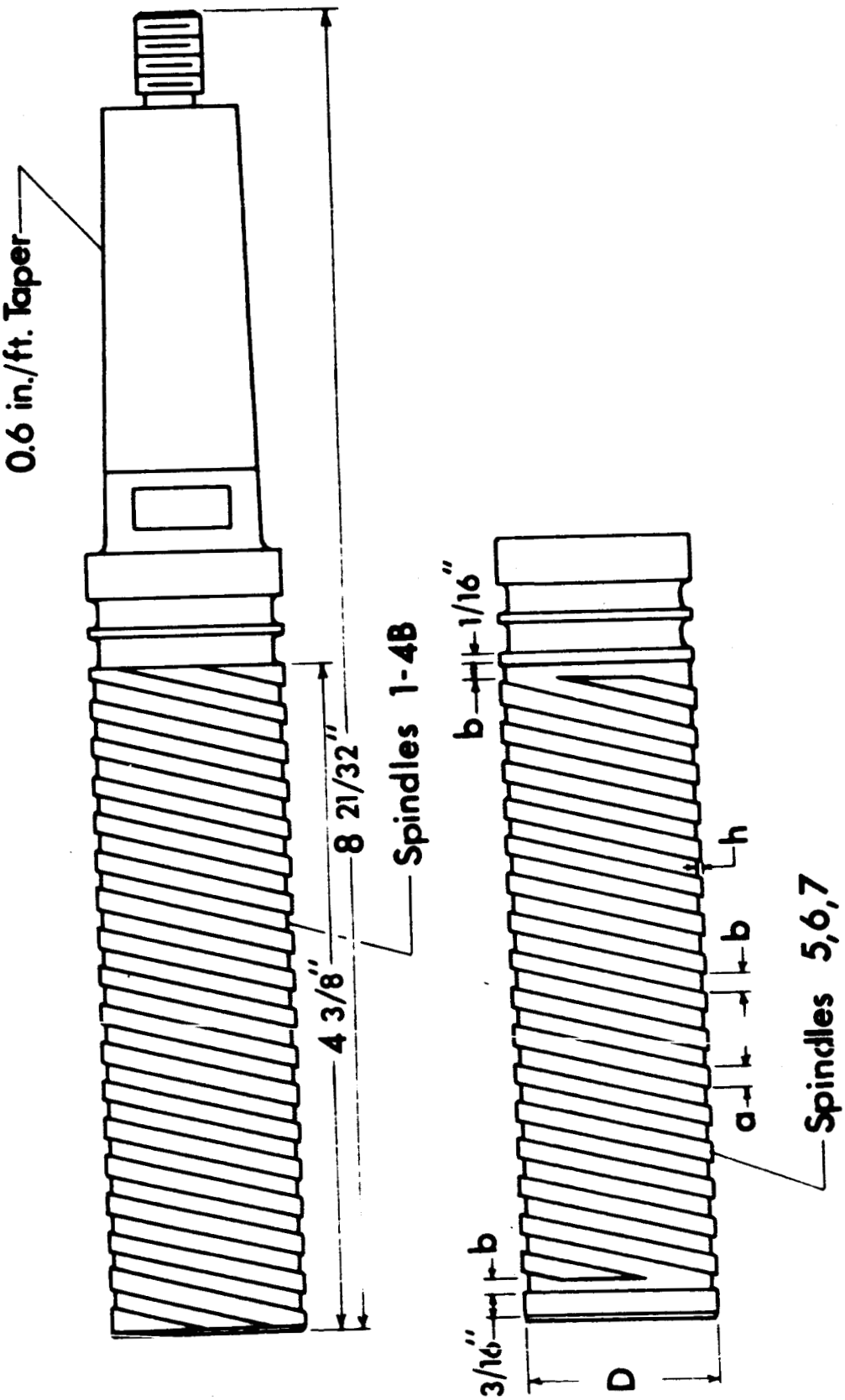

Figure 13. Visco seal test spindles.

order to minimize the end effects, the $\Delta P/L$ was interpreted as dP/dL and evaluated as shown in Figure 12. The viscosity of the test fluid was evaluated at an average temperature determined from the distribution as shown in Figure 12. The temperature variation in the seal was quite small being on the order of 2 degrees F.

CHAPTER IV

EXPERIMENTAL RESULTS

The geometry of spindle number 1 was made similar to the one employed by McGrew and McHugh for the purpose of comparison of experimental results. A geometrical comparison of the two test spindles is shown in Table IV.

During the initial tests of spindle 1, a number of minor problems were encountered. These problems included a ruptured oil filter, a number of pressure tap lines which were quite long and difficult to bleed, a large cavity at the inner end of the test seal which proved to be an air trap, and low sensitivity in the torque measuring bridge. The details of these difficulties and corrections are presented in reference [14]. After modification of the test apparatus, the data compared favorably in the turbulent range, as shown in Figure 14, to the experimental curve of McGrew and McHugh. In the laminar range, however, the value of McGrew and McHugh's experimental curve is higher than the value of the present data, equation (18), or equation (15) which was derived by McGrew and McHugh.

I. SEALING COEFFICIENT

A summary of test results is presented in Table V. Using the theory developed in Chapter II, the theoretical sealing coefficient is compared with the experimental values in Figures 14 through 17.

For all spindles tested Λ_E remained essentially constant during laminar operation. This result is in agreement with equation (18) which indicates that $\Lambda_T \neq f(Re_c)$ in the laminar region. The average ratio of Λ_E to Λ_T for laminar operation is 0.968. During the turbulent operation of each of the seals 2, 3, 4, 2B, 3B, and 4B, the ratio of Λ_E to Λ_T remained essentially constant. However, because of the variation of slopes in the turbulent region for test series 5, 6, and 7, the ratio of Λ_E to Λ_T was not constant.

With the onset of turbulence Λ_E begins to decrease with increasing Reynolds numbers. The Reynolds number at which transition from laminar to turbulent operation occurs is a function of γ. In test series

TABLE IV

COMPARISON OF TEST SCREW GEOMETRIES

Test Seal	α, Degrees	β	γ	c, in.	h, in.	a, in.	b, in.	D, in.
Spindle Number 1	14.5	3.38	0.631	0.0042	0.0101	0.0934	0.1596	1.2430
McGrew and McHugh's Test Spindle	14.5	3.86	0.625	0.0035	0.0100	0.0760	0.1270	0.9940

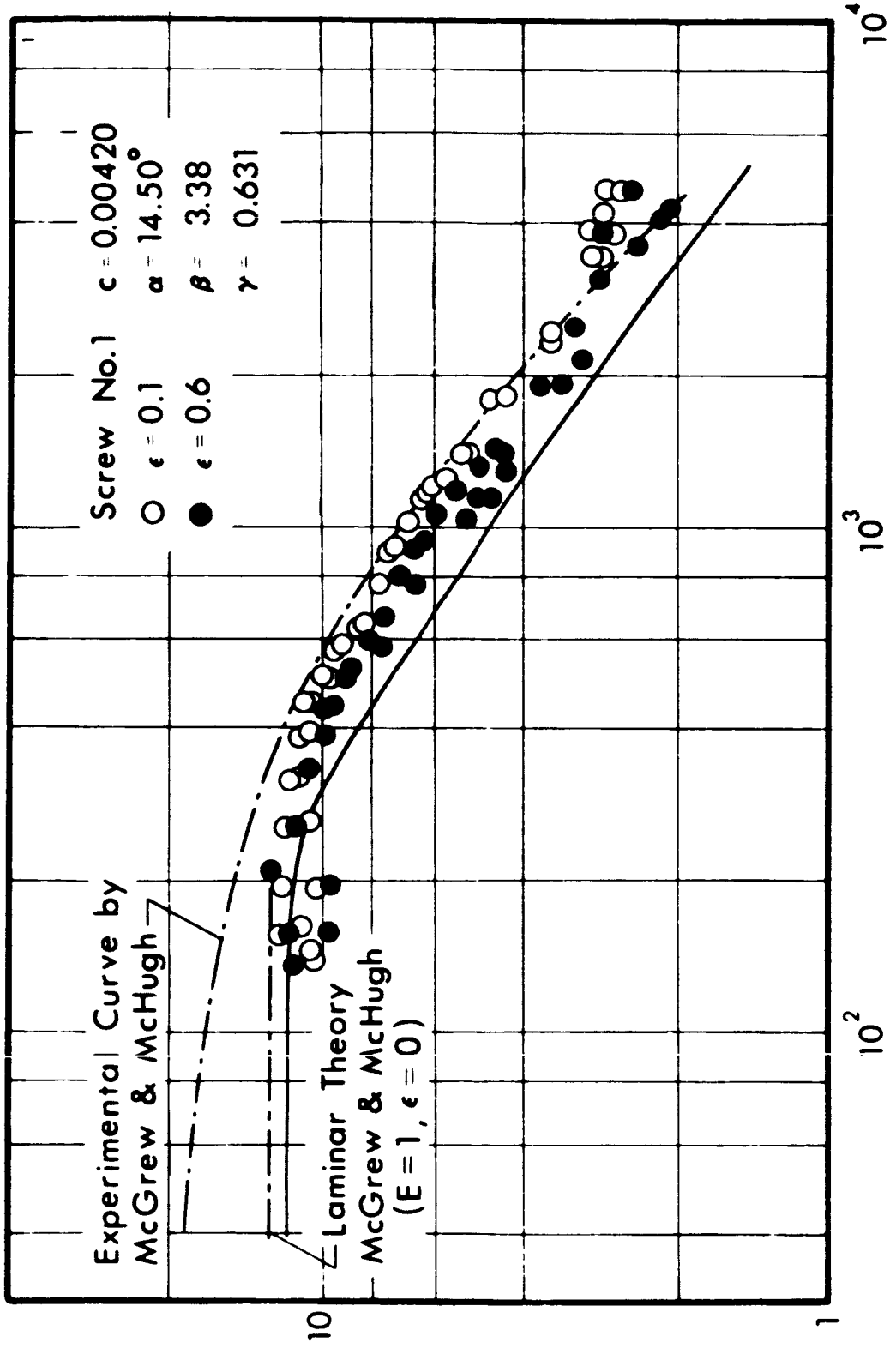

Figure 14. Theoretical and experimental sealing coefficient for spindle 1.

TABLE V

COMPARISON OF TEST RESULTS

Test Seal Number	1	2	3	4	2B	3B	4B	5	6	7
Λ_T (Laminar	11.73	13.09	12.39	12.86	17.54	14.29	17.20	14.08	12.44	14.10
Λ_E (Laminar)	10.98	12.86	12.25	11.62	17.90	16.02	14.40	14.92	11.33	11.75
$\frac{\Lambda_E}{\Lambda_T}$ (Laminar)	0.93	0.98	0.99	0.90	1.02	1.12	0.84	1.06	0.91	0.83
$-\frac{d\,\Lambda_E}{d\,Re_c}$ (Turbulent)	0.698	0.731	0.695	0.676	0.709	0.709	0.709	0.414	0.430	0.438

2, 3, and 4, the three test spindles have essentially the same α, β, c, and D with variations in γ only. Spindle 2, having the lowest γ, resulted in the longest laminar operational region, while spindle 4, with the largest γ, resulted in the shortest operational laminar region, as may be observed in Figure 15. Thus, as γ increases the transitional Reynolds number decreases. The decrease in the transitional Reynolds number, defined in equation (99), is to be expected since the average clearance in the seal is increasing. This direct relationship between the onset of turbulence and γ is in agreement with the theoretical projection in Chapter II.

The relationship between α Λ_E was demonstrated in test series 5, 6, and 7. The geometric parameters of spindles 5, 6, and 7 are essentially the same as for spindles 2, 3, and 4 with the exception of α which was decreased from 9.67° to 5.81°. In tests of seals having α's of 9.67 and 14.5°, the slope of Λ_E, d Λ_E/dR_c, in the turbulent zone was approximately -0.70, which agrees with the theoretical prediction of -0.709. However, for an α of 5.81° the value of d Λ_E/dR_c was found to be approximately -0.43 for the range of experimental data recorded. The relationship between Λ_T and α is demonstrated in Figure 18. In this figure it is observed that Λ_T, for α equal to 5.81°, remains laminar to a Reynolds number of 300, while for α equal to 20.15°, Λ_T begins to decrease at a Reynolds number of approximately 100. Therefore, as α increases the transition point from laminar to turbulent operation for Λ_T decreases. However, it is noted from Figure 18 that, for either large or small α's, the predicted slope, d Λ_T/dRe_c, for Reynolds numbers greater than 1000, is the same. In this regard Λ_E and Λ_T do not agree.

The effect of β on Λ_E may be observed in Figures 19, 20, and 21. In series 2B, 3B, and 4B α and γ remain unchanged from series 2, 3, and 4, while β was decreased from approximately 7 to 3. Λ_E for 2B, 3B, and 4B is, on the average, 1.29 times the values for spindles 2, 3, and 4 in both laminar and turbulent operation. This ratio compares favorably with theoretical predictions which indicate that the ratio should be 1.28.

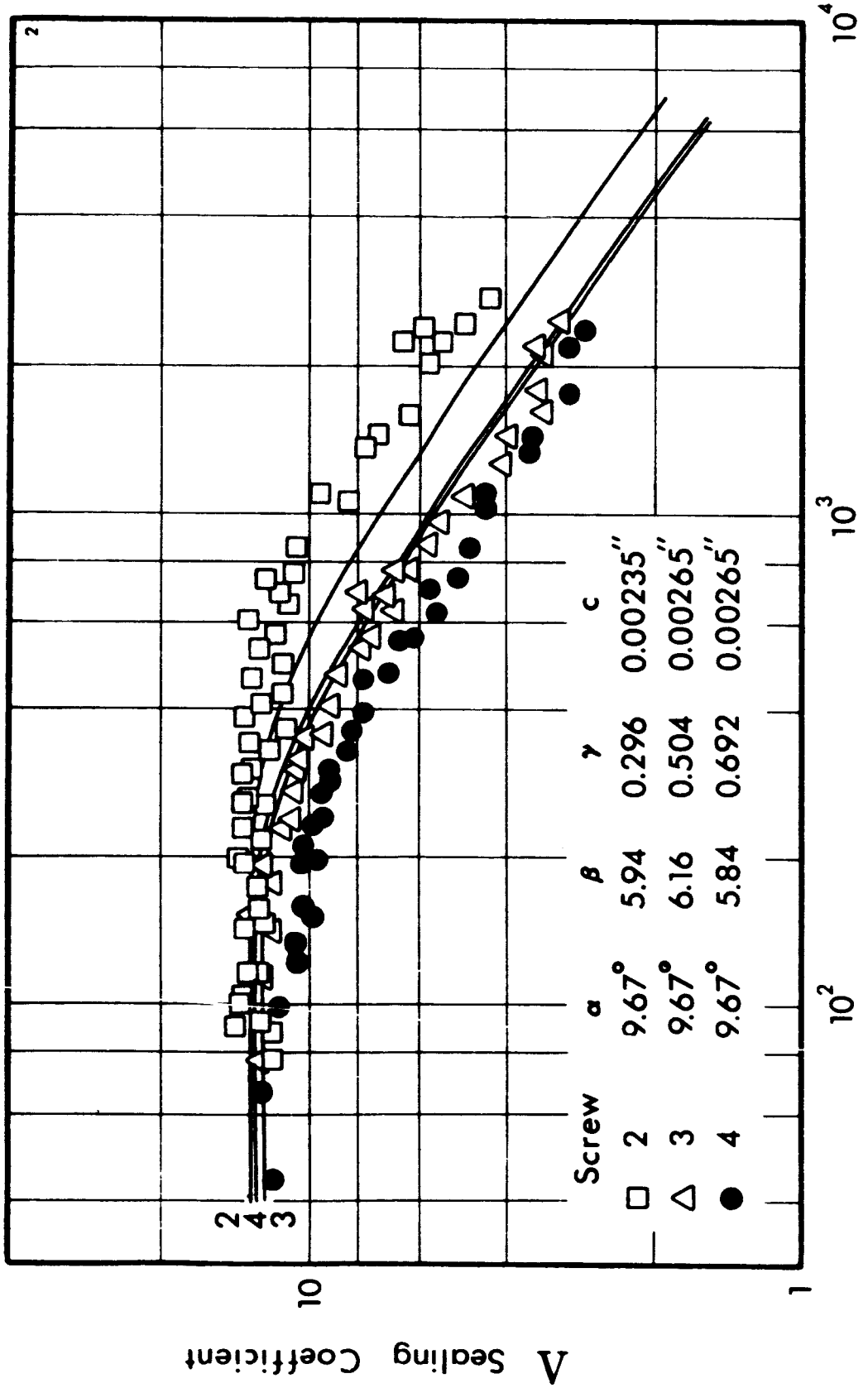

Figure 15. Theoretical and experimental sealing coefficient for spindles 2, 3, and 4.

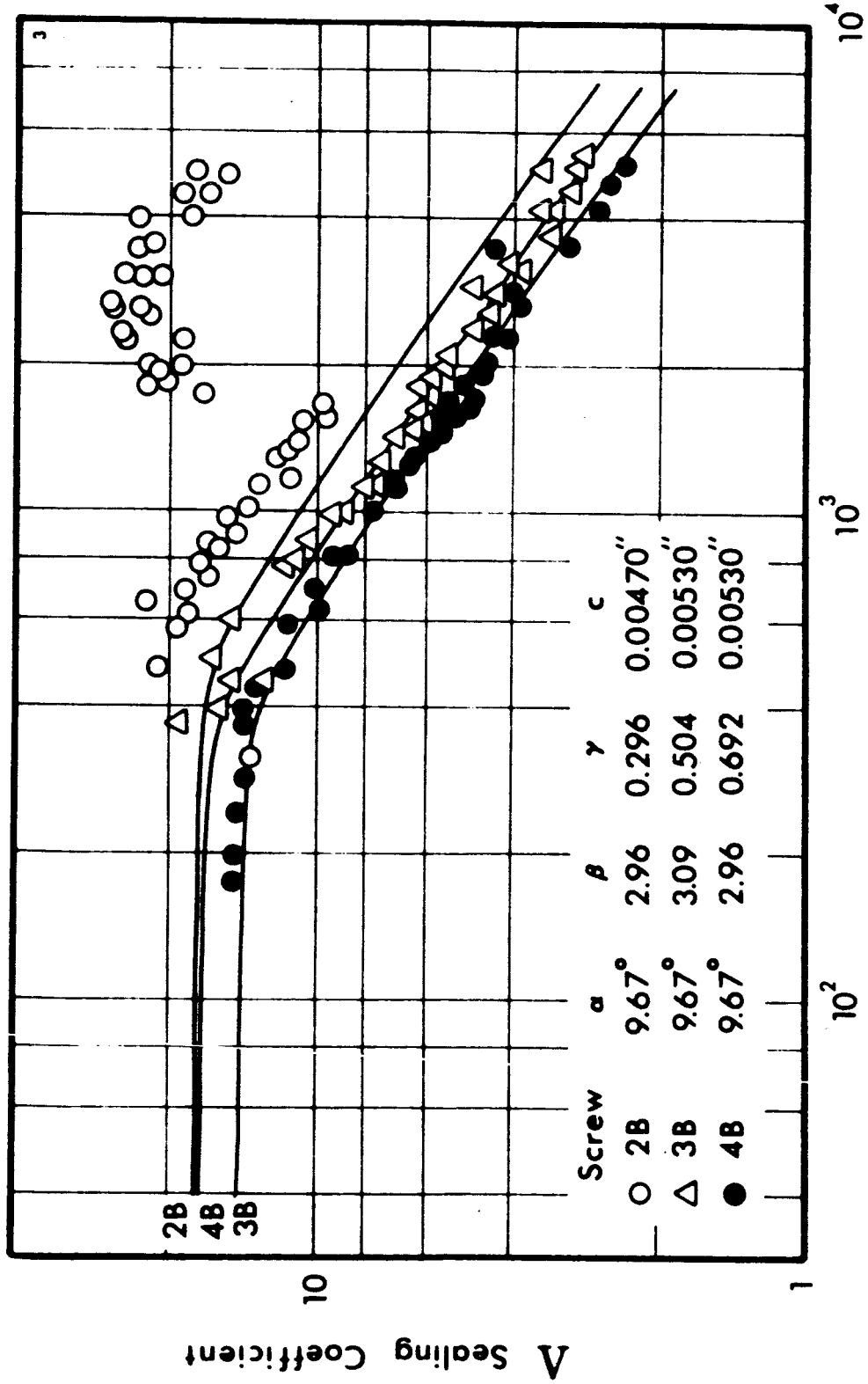

Figure 16. Theoretical and experimental sealing coefficient for spindles 2B, 3B, and 4B.

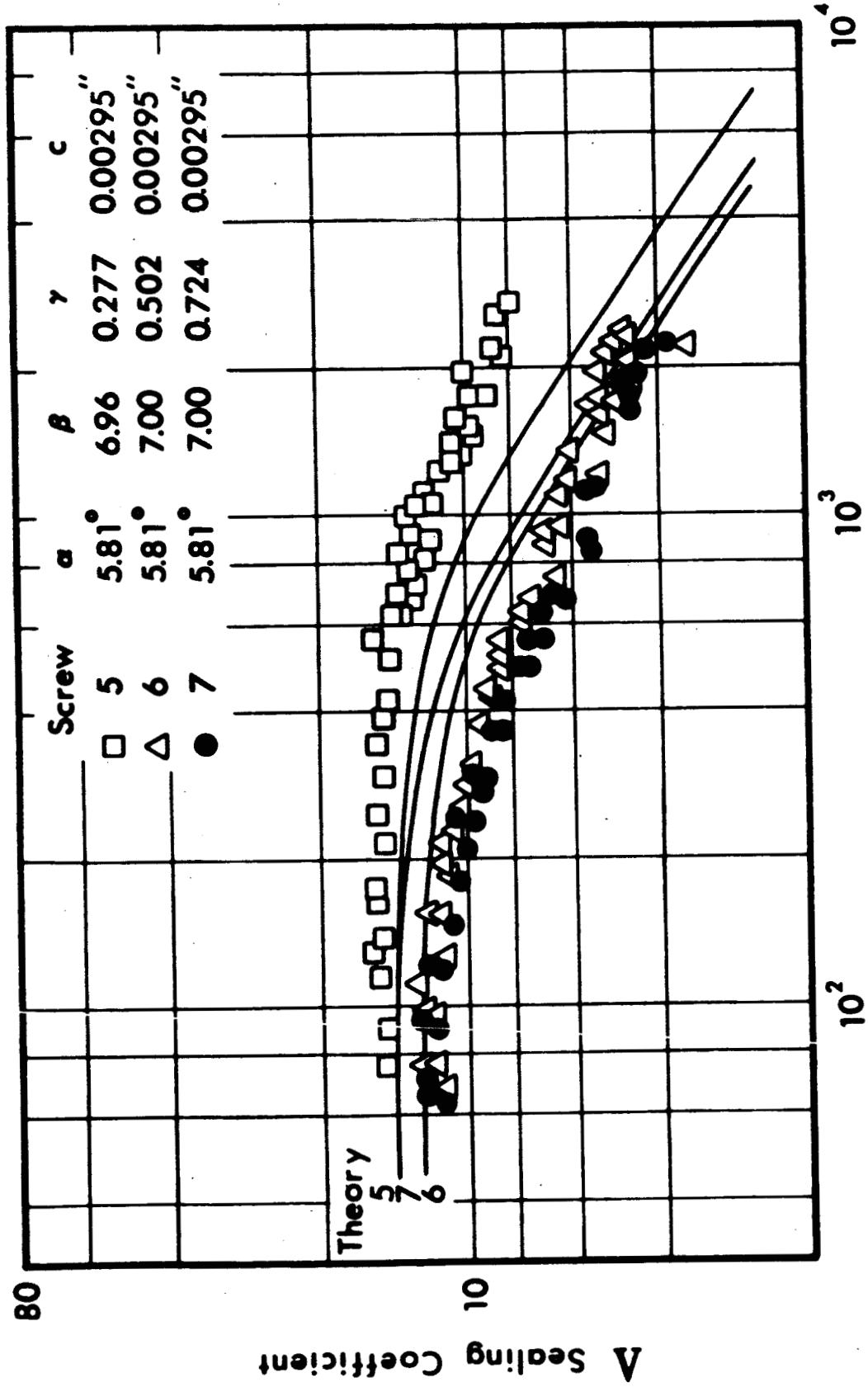

Figure 17. Theoretical and experimental sealing coefficient for spindles 5, 6, and 7.

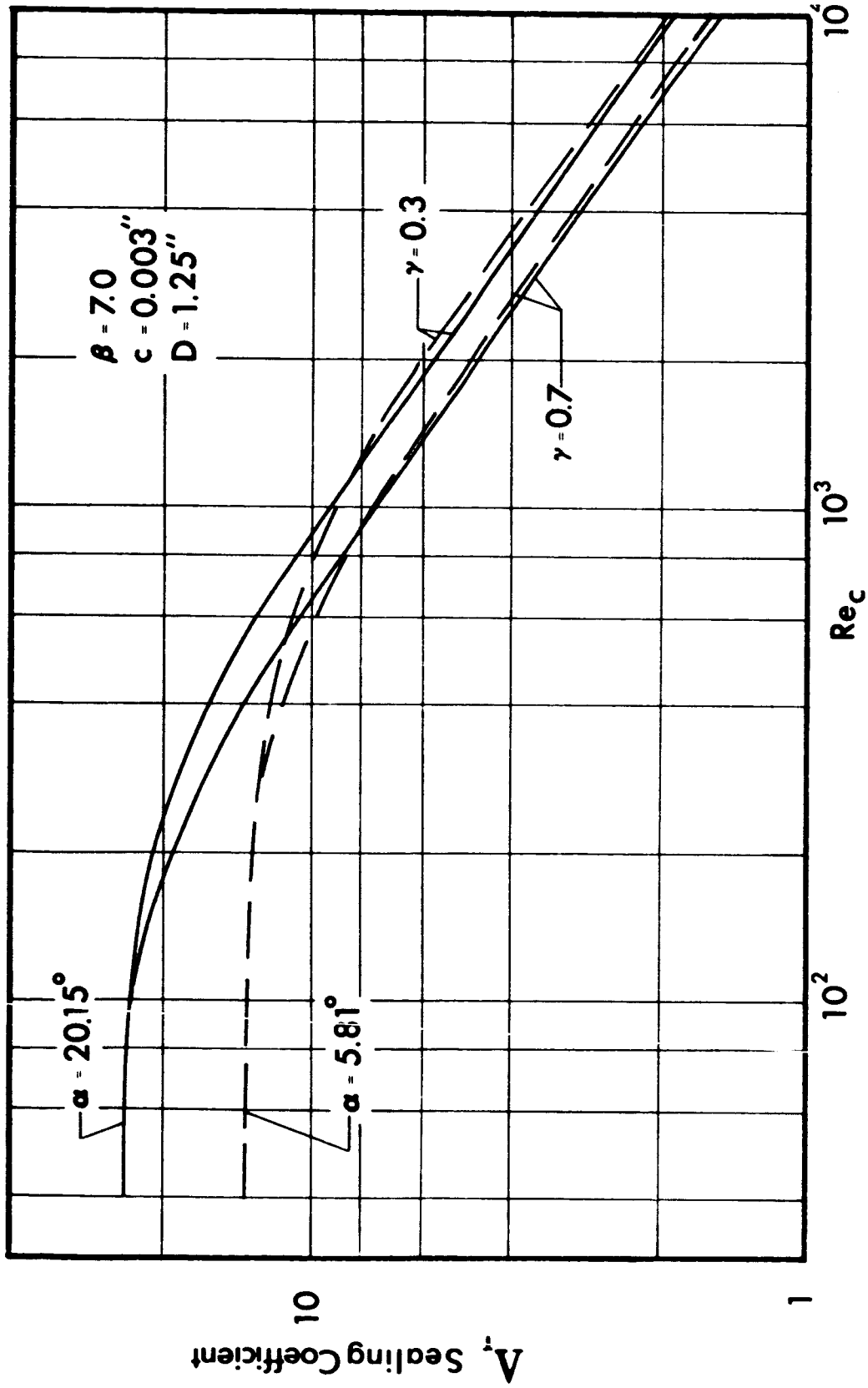

Figure 18. Theoretical sealing coefficient versue Re_c for α of 5.81° and 20.15° with γ of 0.3 and 0.7.

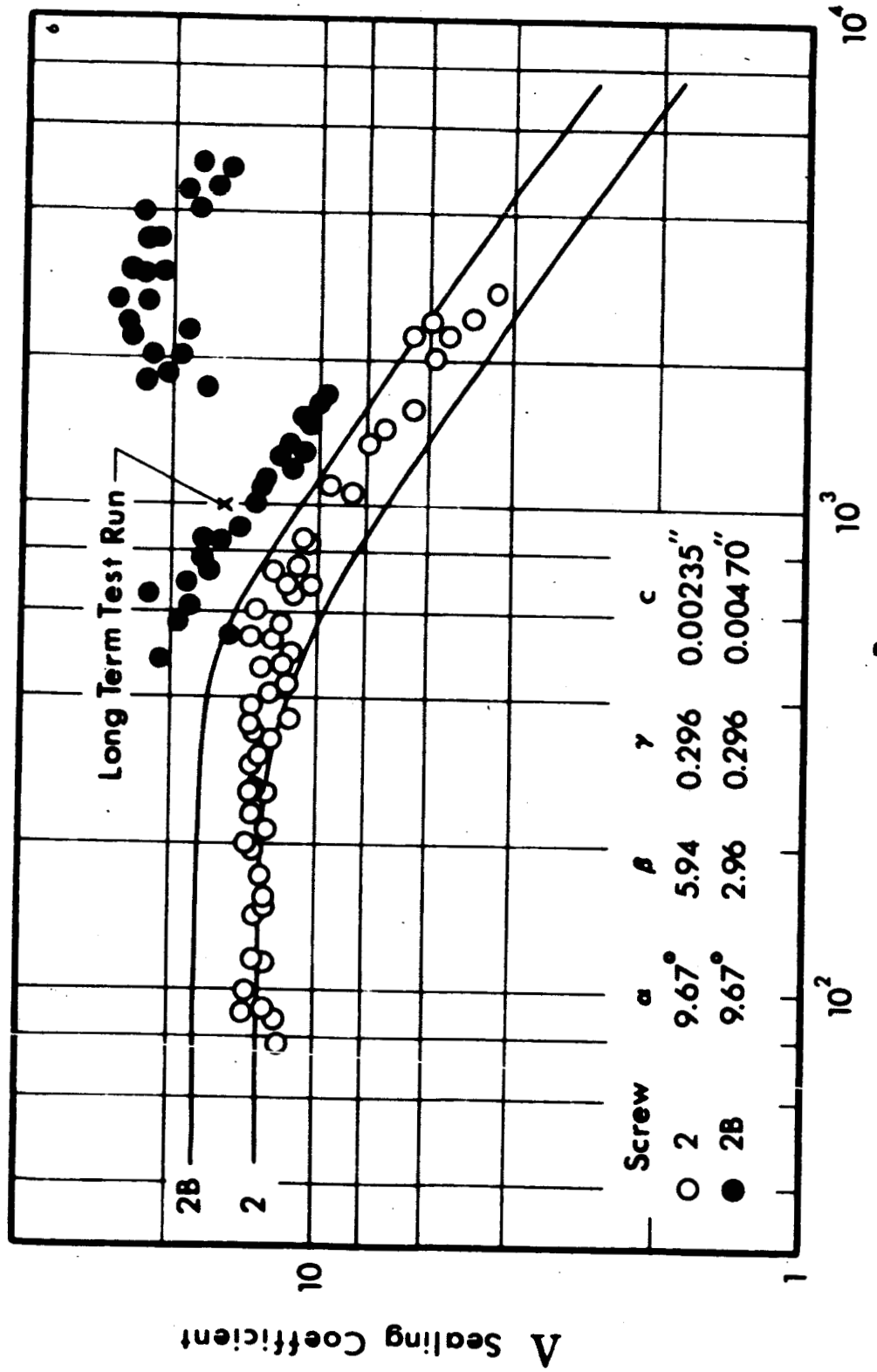

Figure 19. Theoretical and experimental sealing coefficient for spindles 2 and 2B.

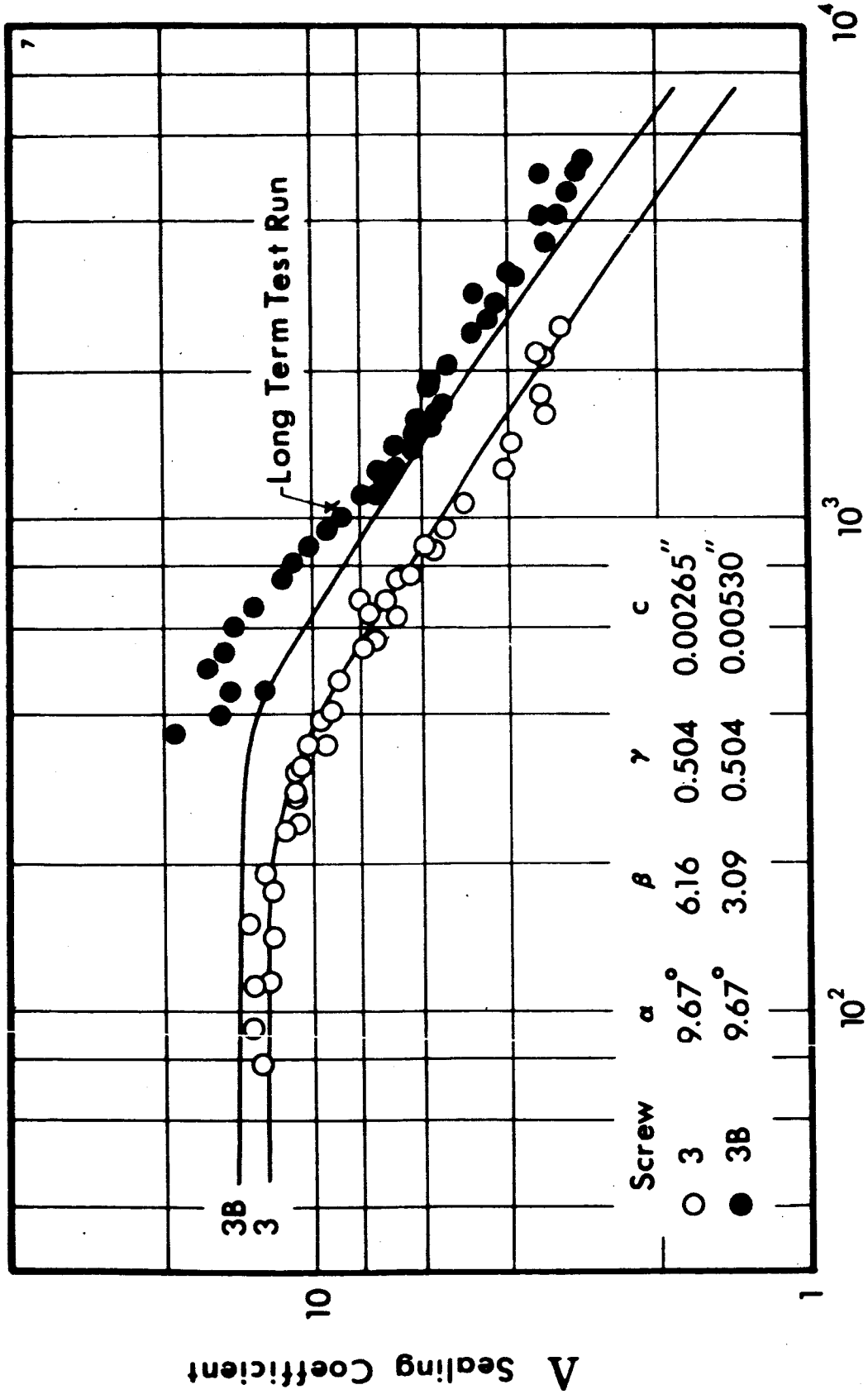

Figure 20. Theoretical and experimental sealing coefficient for spindles 3 and 3B.

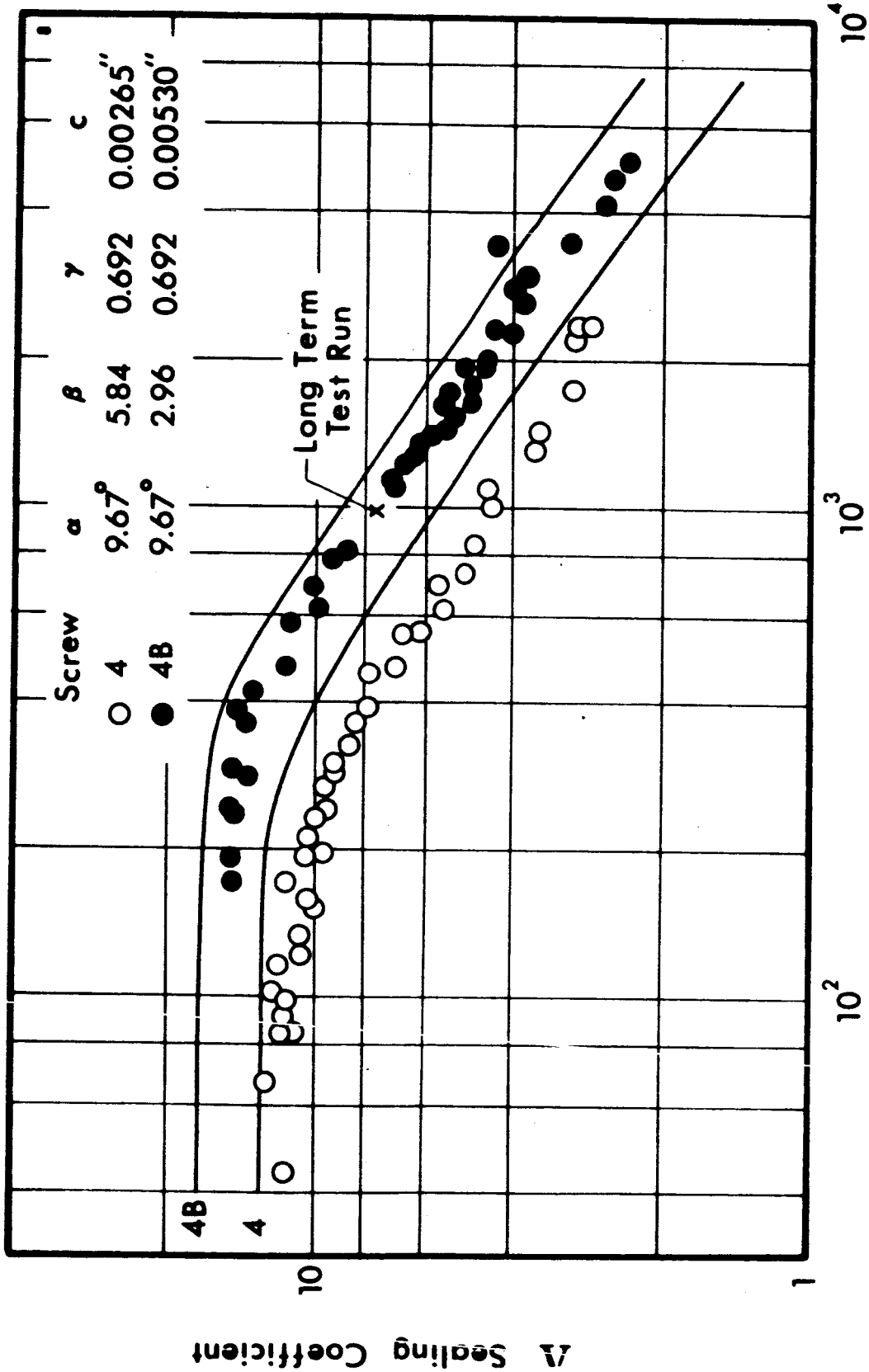

Figure 21. Theoretical and experimental sealing coefficient for spindles 4 and 4B.

In test series 2B there is a sudden large increase in Λ_E at a Reynolds number of approximately 1600. This discontinuity in Λ_E is believed to be the result of air ingestion which produces a decrease in the value of β. A similar observation was made for spindles 3B and 4B, but the perturbation was much lower in magnitude.

A forecast of Λ_T for test spindles 5A, 6A, and 7A, which have yet to be tested, is shown in Figure 22.

II. FRICTION PARAMETER AND DISSIPATION FUNCTION

The power loss in the visco seal during laminar operation was described by Stair in terms of a dissipation function defined by the equation:

$$\phi = 1 - \gamma + \frac{\gamma}{\beta} + 3\,\frac{t^2\,\gamma\,(1-\gamma)\,(\beta-1)^2(1-\gamma+\gamma\beta^3)}{\beta^3\,(1+t^2)+t^2\,\gamma\,(1-\gamma)\,(\beta^3-1)^2}\quad , \tag{105}$$

$$\phi = \frac{qc}{\pi\,\mu\,D\,L\,U^2}\quad , \tag{106}$$

where q is the power loss. The dissipation function depends upon α, β, and γ and is independent of rotational speed. The friction parameter may be defined in terms of the dissipation function as:

$$F.P. = \frac{4\pi\phi}{Re_c}\quad . \tag{107}$$

Thus, F.P. is a function of the seal parameters and speed. The laminar experimental data for the friction parameter are in agreement with equation (107) as shown in Figures 23, 24, and 25. The experimental data in the turbulent range follows the trend noted by Smith and Fuller [16] whose data for the friction parameter of a plain journal bearing operating under laminar and turbulent conditions can be expressed as:

$$F.P._{\ell} = 4\,\pi/Re_c, \tag{108}$$

and

$$F.P._{\circ} = 0.156\,\pi/Re_c^{\,0.43}\quad . \tag{109}$$

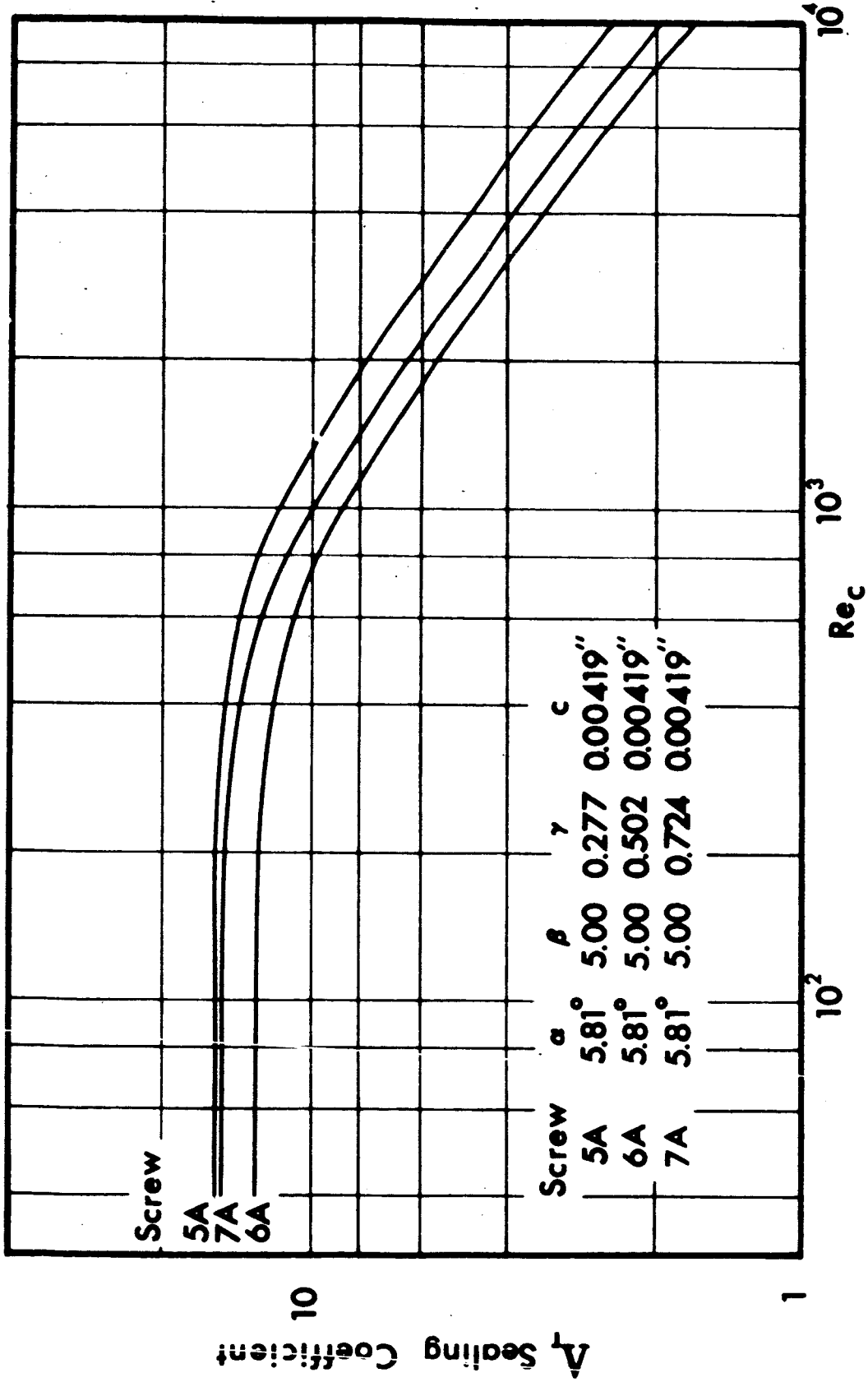

Figure 22. Theoretical sealing coefficient for spindles 5A, 6A, and 7A.

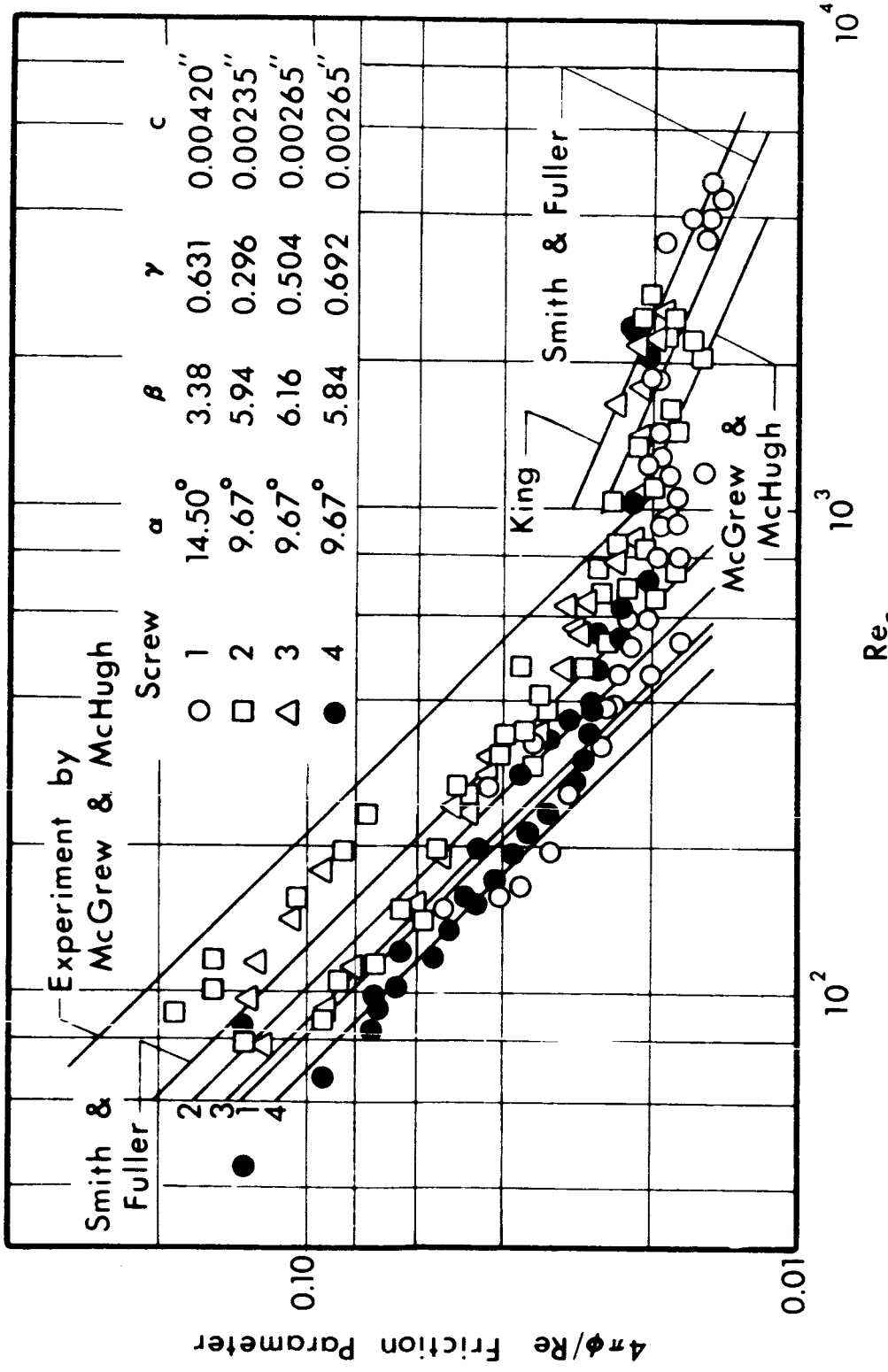

Figure 23. Theoretical and experimental friction parameter for spindles 1, 2, 3, and 4.

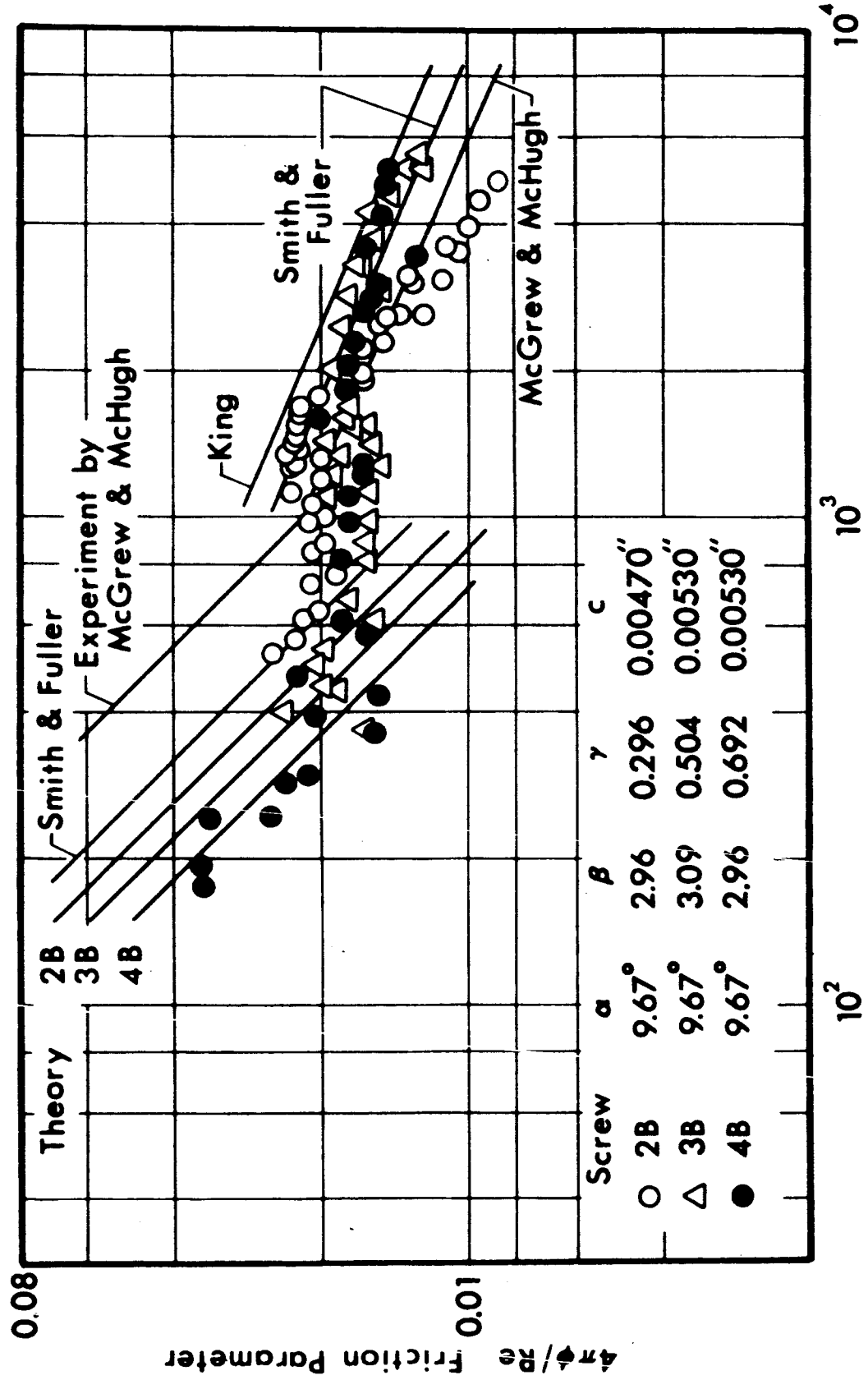

Figure 24. Theoretical and experimental friction parameter for spindles 2B, 3B, and 4B.

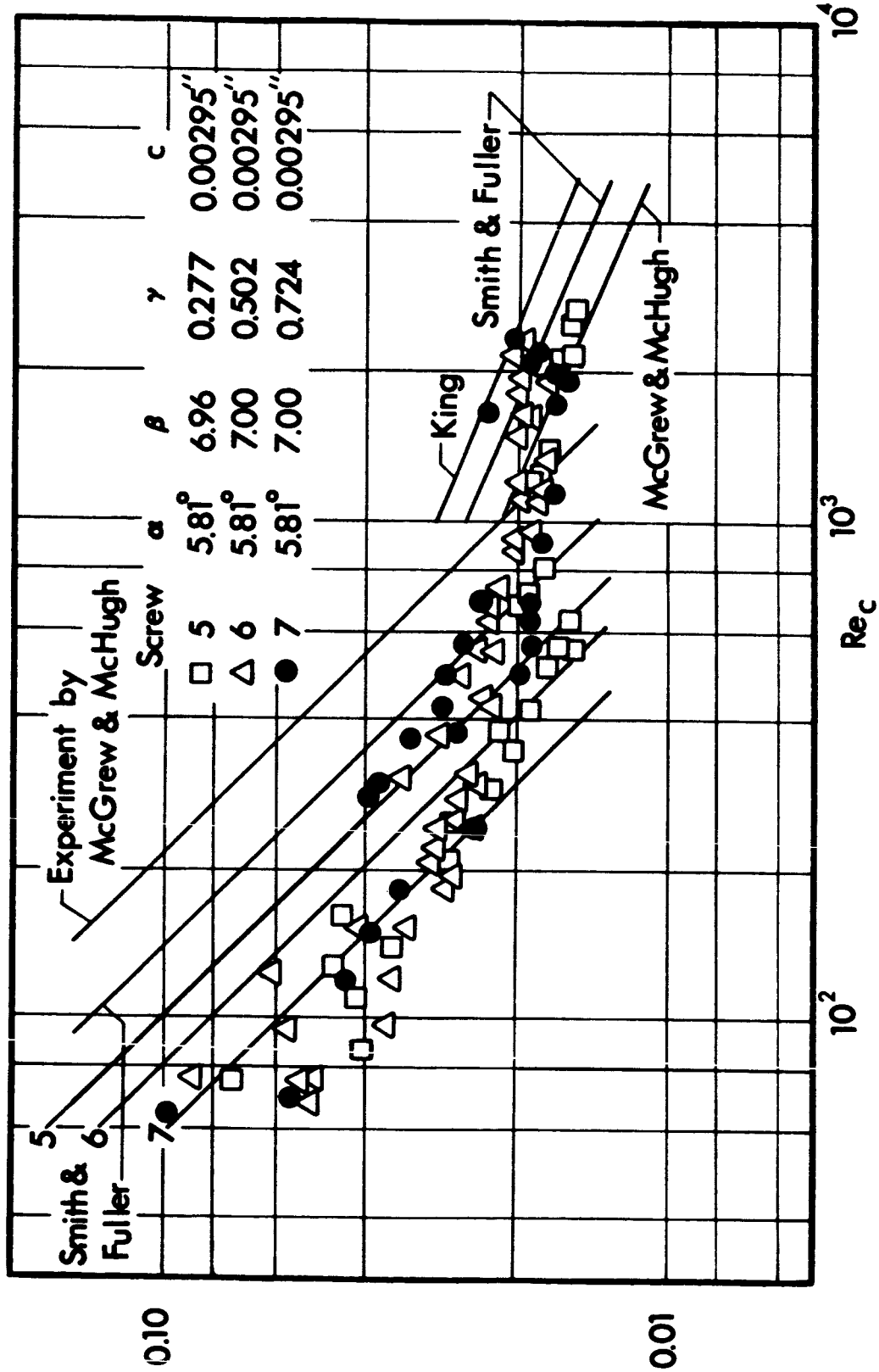

Figure 25. Theoretical and experimental friction parameter for spindles 5, 6, and 7.

As the visco seal more nearly approaches a journal bearing, γ becoming smaller, the experimental data for the friction parameter approaches the laminar experimental curve presented by Smith and Fuller. In the turbulent region, however, the experimental data for the seal is approximately 1.051 times that of Smith and Fuller's. Thus, in laminar operation the friction parameter is described by equation (107) and during turbulent operation Smith and Fuller's turbulent journal bearing results can be utilized to estimate the friction parameter.

III. AIR INGESTION

The phenomenon designated "seal break" by McGrew and McHugh and "secondary leak" by King was not observed directly during this experimental study. The term "seal break" refers to a small leak past the seal interface. However, in the present series of tests, a phenomenon which has been termed "air ingestion" was quite evident. Air ingestion is a condition in which air is forced, by the action of the screw exposed to air, through the seal interface into the seal. During laminar operation air ingestion was not observed. However, as the speed and degree of turbulence increased, air bubbles began to rise in the pressure tap lines. Continuous bleeding would not remove the entrapped air from the system once the condition of air ingestion was present. Air ingestion tended to decrease the pressure gradient near the atmospheric end of the seal, which, in turn, increased the effective length of the seal. The seal would not leak unless the effective seal length required to maintain the seal supply pressure became longer than the actual seal length or pressure fluctuations caused a slug of fluid to be discharged.

Air ingestion was found to be related to the surface wetability and Reynolds number of the seal. In a test series for spindle 1, in which wetting conditions were present, the air ingestion became severe leading to pulsating pressures which caused the series to be stopped. It was observed that air ingestion and seal instability during this test began at a much lower Reynolds number than in previous tests. Care was taken in all later tests to insure that the condition of shaft wetting did not reoccur by coating all

test spindles with a very thin film of oil.

Air ingestion may have a pronounced effect on Λ_E in the turbulent region under certain operational conditions. In series 2B, Figure 16, it is postulated that air ingestion, by displacing fluid at the root of the grooves, caused a decrease in β with a consequent increase in Λ_E, as demonstrated in Figure 26. As shown in Figure 7, for a Reynolds number of 1000 and $\beta \simeq 3$, a small decrease in β produces a large increase in the value of Λ_T. This same discontinuity was observed to a smaller degree in the data for spindle 3B and smaller yet in spindle 4B. While the β for 3B and 4B were similar to that for 2B, the groove widths were greater. It is believed that the wider grooves made the displacement of liquid from the root of the groove more difficult and this prevented the change in Λ_E from being as great as in 2B. As long as the seal's operational point is located along the flat portions of the curves in Figures 6 through 9, a change in β due to air ingestion produces only a small change in the sealing coefficient. Also, the larger the value of γ, the lower the change in β when air ingestion is present. In order to minimize the effects of air ingestion and improve seal stability, it appears desirable to select the seal geometry with a low α, high γ, and large β values as suggested in Figures 6 through 9.

IV. LONG TERM SEAL OPERATION

To insure the feasibility of operating the visco seal for extended periods of time, a series of long term tests of one to two hours duration were conducted for each of the spindles, beginning with 2B. In each case equilibrium was reached in 15 to 20 minutes of seal operation. No seal leakage was observed during these long term tests and air ingestion was not observed in laminar operation. In each of the turbulent tests air ingestion was observed to some degree. However, a Reynolds number was reached where it appeared that long term operation of the seal was not desirable. The maximum Reynolds number at which the seal can operate in an equilibrium condition in the turbulent zone is related to the spindle parameters. Further experimental studies are needed before definite conclusions can be made regarding the

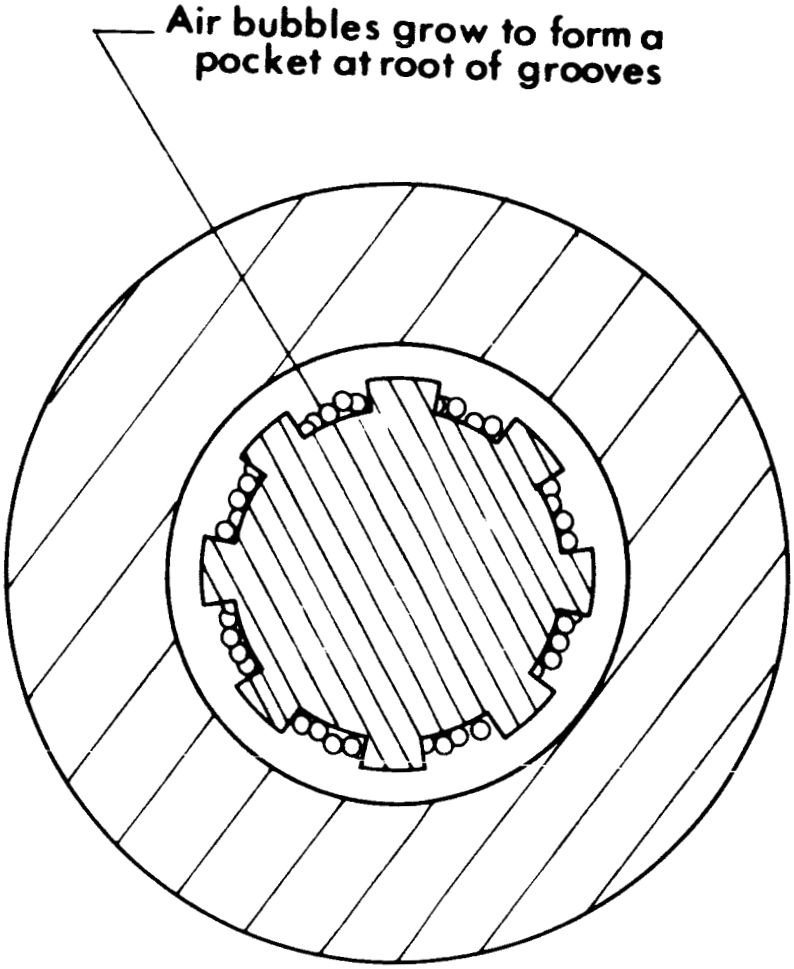

Figure 26. Schematic representation of the change in β due to air ingestion.

maximum speed.

V. OTHER EXPERIMENTAL RESULTS

The effect of the eccentricity ratio on Λ_T was predicted by McGrew and McHugh in equation (15) to vary as E varies from 1 to 2.5 for eccentricity ratios of 0 to 1. For laminar operation, however, Λ_E, in the absence of air ingestion was found to be essentially independent of the eccentricity ratio, while in turbulent operation Λ_E was noted to decrease slightly with an increase in eccentricity ratio as can be observed in Figure 14. It appears, therefore, unnecessary to incorporate the eccentricity ratio as a significant variable in the equation for Λ_T in the laminar range. It was noted, however, that eccentric operation of the seal in the turbulent range tended to increase air ingestion.

In Figure 27 the experimental data taken from a series of tests conducted by King, along with Λ_T computed by equation (97) for the thread geometry used by King, are shown. The predicted sealing coefficient is in good agreement with the 5D and 2E series of data in the turbulent range. In the laminar range the predicted value for the sealing coefficient is smaller than King's extrapolated data curves. It is difficult to draw conclusions about the laminar zone since King obtained limited data in this region. In series 3C and 1B, the slopes of King's experimental sealing coefficients are -0.527 and -0.466, agreeing with the slopes of Λ_E in test series 5, 6, and 7. Data curves 5D and 2E have slopes in the turbulent region of -0.706 and -0.686, which are similar to the values obtained in test with spindles 1 through 4B, as discussed in Chapter IV. From the experimental evidence reported in this work, along with data from King, the indication is that for small helix angles, 3° to 6°, the initial slope of the experimental sealing coefficient in the turbulent zone is approximately -0.46. For helix angles of 7° to 14° corresponding to the range of optimum α recommendations of various investigators, the slope of the experimental sealing coefficient is approximately -0.70.

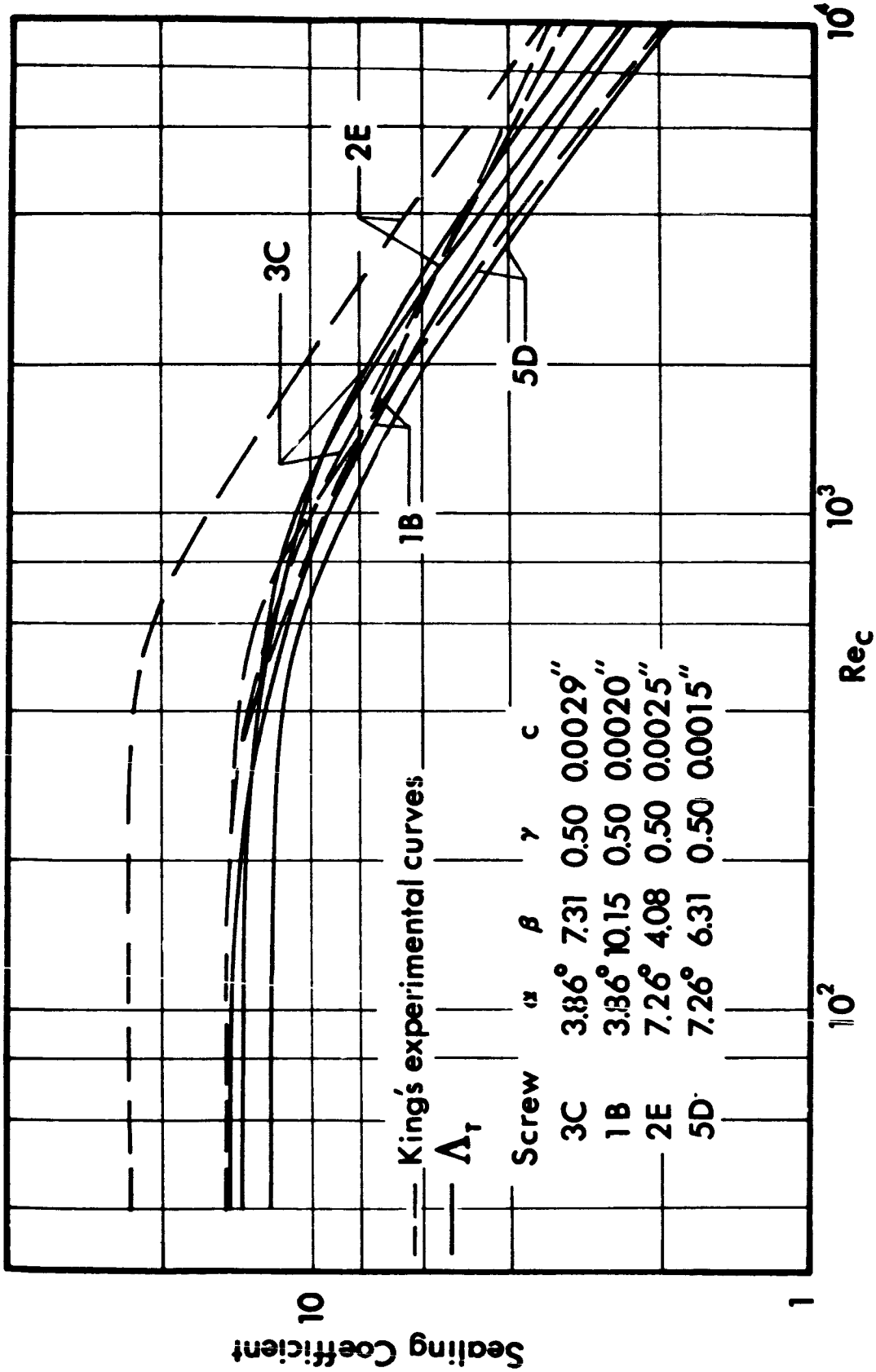

Figure 27. Comparison of King's experimental data with the theoretical sealing coefficient.

CHAPTER V

CONCLUSIONS AND RECOMMENDATIONS

Based on the analytical laminar analysis of the visco seal developed by Boon and Tal, equations were derived to predict the operation of the visco seal in the laminar and turbulent regions. The theoretical sealing coefficient developed by this analysis was compared with the experimental sealing coefficient obtained for ten experimental seals. In view of the observations and comparisons presented in this work, the following conclusions are indicated:

1. The laminar analysis leading to equation (18), upon which the present analysis is based, agrees more closely with the experimental results in laminar flow than any of the other analytical approaches considered.

2. The optimum screw geometry for laminar operation was not optimum for operation in the turbulent range.

3. For screws which must operate in both the laminar and turbulent range, smaller helix angles will provide more flexible operation in both regions.

4. In turbulent operation the visco seals having small helix angles operate with a greater degree of pressure stability.

5. Experimental Λ is essentially constant in laminar operation and in agreement with equation (18).

6. The transition Reynolds number at which Λ_E begins to decrease, decreases with increasing γ and is in agreement with equation (99).

7. The slope of Λ_E in the turbulent range for helix angles of 9.67° and 14.5° was approximately -0.70, while this value decreased to -0.43 for helix angles of 5.81°.

8. The phenomenon of air ingestion will be encountered in turbulent operation. This condition was observed to be a function of shaft wetability, Reynolds number, seal geometry, and eccentricity ratio, but until more experimental data are obtained this relationship cannot be precisely defined.

However, in order to minimize the effects of air ingestion on Λ_E, large β and γ along with small α should be employed.

9. An attempt was made in test series 5, 6, and 7 to alleviate the problem of air ingestion. End dams, as shown in Figure 13, were added to minimize the condition, although the end result was not as effective as was expected. The decrease in air ingestion was slight necessitating the conclusion that more data are needed before a concrete relationship between end dams and air ingestion can be determined.

10. There exists a maximum Reynolds number beyond which long term operation is no longer feasible. However, more experimental data are needed before this value can be precisely defined.

11. The frictional losses in the visco seal may be described with existing equations. In the laminar range the theoretical predictions by Stair closely approximate the experimental data. During turbulent operation the experimental data presented by Smith and Fuller, represented by equation (109), are 0.951 times the value of the friction parameter observed in these tests. Therefore, the frictional losses in the seal may be calculated either for laminar or turbulent operation by:

$$F.P._{\ell} = 4\pi\Phi/Re_c \ ,$$

and

$$F.P._o = 0.164\pi/Re_c^{0.43} \ .$$

12. For laminar operation Λ_E is essentially independent of ϵ and under turbulent conditions the effect of seal eccentricity is slight.

A number of aspects of the visco seal operation in the turbulent range require further and more intensive study. Specific problem areas requiring additional attention are as follows:

1. More experimental data in the turbulent range for Reynolds numbers higher than 3000 are needed in order to determine the maximum Reynolds number for long term seal operation.

2. The construction of test spindles with helix angles of approximately 5° and β's in the range from 10 to 20 are needed in order to verify the observations discussed in Chapter II concerning the relatively small effect of β on Λ_T for high Reynolds numbers and small helix angles.

3. A refinement of equation (97) for the calculation of Λ_T is needed in order to better describe the sealing coefficient in the turbulent region for small helix angles. It is realized that the two lines in Figure 5 may not be the best estimate for all geometric parameters.

4. An investigation of the effects of grooves located in the housing rather than along the shaft would be desirable. This is based on the assumption that a smooth shaft located in the threaded housing would lessen the effects of air ingestion on Λ_E.

LIST OF REFERENCES

LIST OF REFERENCES

1. Rowell, H. S., and Finlayson, D. "Screw Viscosity Pumps," Engineering, Vol. 126, August 31, 1928, pp. 249-250, Sept. 28, 1928, pp. 385-7.

2. Whipple, R. T. P. "Theory of the Spiral Grooved Thrust Bearing With Liquid or Gas Lubricant," U.K.A.E.A., Atomic Energy Research Establishment, T/R 622, March 6, 1951.

3. Hughes, D. P. "Shaft Seal for High Gas Pressure," International Conference on Fluid Sealing, Paper C1, B.H.R.A., April 17-19, 1961, Harlow Essex, England.

4. Zotov, V. A. "Research on Helical Groove Seals," Russian Engineering Journal Translation, Vol. 10, October 1959, pp. 3-7.

5. Frossel, W. "Hochtourige Schmierolpumpe," Konstruction, Vol. 12, No. 5, 1960, pp. 195-203.

6. Asanuma, T. "Studies on the Sealing Action of Viscous Fluids," "International Conference on Fluid Sealing," Paper A3, B.H.R.A., Harlow Essex, England.

7. McGrew, J. M., and McHugh, J. D. "Analysis and Test of the Screw Seal in Laminar and Turbulent Operation," The General Electric Advanced Technology Laboratories, Report No. 63GL66, May 3, 1963.

8. King, A. E. "Engineering Information Report on Tests Made With a Hydrodynamic Screw Seal (Viscoseal) in Oil, Water, and Potassium" Westinghouse Electric Corporation, Aerospace Electrical Division, Report No. WAED 63.3 (Revision A), September, 1964.

9. Boon, E. F., and Tal, S. E. "Hydrodynamische Dichtung fur rotierende Wellen," Chemie-Ing-Technik, Vol. 31, No. 3, January 31, 1959, pp. 202-212.

10. Stair, W. K. "Analysis of the Visco Seal--Part 1, The Concentric Laminar Case," Mechanical and Aerospace Engineering Research Report ME 65-587-2, University of Tennessee, January 18, 1965.

11. Pai, S. I. Viscous Flow Theory, II, Turbulent Flow, D. Van Nostrand Company, New York, 1957, pp. 33-37.

12. Laufer, J. "Some Recent Measurements in a Two-Dimensional Turbulent Channel," Journal of Aeronautical Science, Vol. 117, No. 5, 1950, pp. 277-287.

13. Pinkus, O., and Sternlicht, B. Theory of Hydrodynamic Lubrication, McGraw-Hill Book Company, New York, 1961, pp. 368-371.

14. Bowman, C. F. "The Design and Construction of a Visco Seal Test Facility," Mechanical and Aerospace Engineering Research Report ME 66-587-6, The University of Tennessee, June 1966.

15. Smith, M. I., and Fuller, D. D. "Journal-Bearing Operation at Superlaminar Speeds, "Trans. of A.S.M.E., Vol. 78, 1956, pp. 469-474.

APPENDICES

APPENDIX A

SAMPLE CALCULATIONS

Equation (97) is the theoretical sealing coefficient for both laminar and turbulent operation for the visco seal. In order to calculate the sealing coefficient, the geometric configuration of the seal is needed. For this example the parameters of test spindle 1 will be used. Hence:

$\alpha = 14.5°$

$t = 0.2586$

$\beta = 3.38$

$\gamma = 0.631$

$c = 0.0042$ in.

and

$D = 1.2430$ in.

From these data, I_1, I_2, I_3, and I_4 in equation (97) are evaluated as:

$$I_1 = (1 - \gamma)\, t^2 = 0.0246,$$

$$I_2 = \beta^3 \gamma\, t^2 = 1.635,$$

$$I_3 = \frac{\beta^3}{\gamma + \beta^3 (1 - \gamma)} = 2.595,$$

and

$$I_4 = t \left[1 - \gamma + \gamma\beta - \frac{\gamma + \beta^3 (1 - \gamma) + \gamma(\beta - 1)}{\gamma + \beta^3 (1 - \gamma)} \right] = 0.364.$$

The critical Reynolds number defined by equation (99) is:

$$Re_{crit.} = 41.1 \left[\frac{D/2}{(1 - \gamma)\, c + \gamma \beta\, c} \right]^{1/2} = 317.$$

When the operation of the seal is laminar, F_ξ and F_η are both unity. The terms K_4 and K_5, in equation (97), can be calculated as:

$$K_4 = \frac{3}{2F_\xi}\left[1 - \frac{F_\xi}{10.5\,F_\xi - 7.5} + \frac{1 - F_\xi}{3.92\,F_\xi^2 - 1.4\,F_\xi - 1}\right] = 1$$

and

$$K_5 = \frac{3}{2F_\eta}\left[1 - \frac{F_\eta}{10.5\,F_\eta - 7.5} + \frac{1 - F_\eta}{3.92\,F_\eta^2 - 1.4\,F_\eta - 1}\right] = 1$$

Therefore, the predicted sealing coefficient for laminar operation becomes:

$$\Lambda_T = K_4\left(\frac{I_1 + I_2}{I_4}\right) + K_5\left(\frac{I_3}{I_4}\right) = 1\,(4.50) + 1\,(7.23) = 11.73,$$

which is the same value as obtained from equation (18). When the flow in the seal becomes turbulent, F_ξ and/or F_η is greater than 1. Therefore, F_ξ is evaluated from Figure 5 as:

$$F_\xi = \left(\frac{f_o}{f_\ell}\right)_\xi = \frac{0.326\,Re_p}{64\,Re_p^{0.253}} = 0.00509\,Re_p^{0.747},$$

or substituting for Re_p from equation (103),

$$F_\xi = 0.00509\left[2000\,\cos\alpha\,\frac{Re_c}{Re_{crit.}}\right]^{0.747}.$$

Similarly,

$$F_\eta = 0.0101\left[2000\,\sin\alpha\,\frac{Re_c}{Re_{crit.}}\right]^{0.754}.$$

Assume $Re_c = 400$. Therefore,

$$F_\xi = 0.00509\left[2000\,\cos 14.5\,\frac{400}{317}\right]^{0.747} = 1.755$$

and

$$F_{\eta} = 0.0101 \left[2000 \sin 14.5 \left(\frac{400}{317}\right)\right]^{0.754} = 1.293$$

from which

$$K_4 = \frac{3}{2(1.755)} \left[1 - \frac{1.755}{10.5(1.755) - 7.5} + \frac{1 - 1.755}{3.92(1.755)^2 - 1.4(1.755) - 1}\right] = 0.639$$

and

$$K_5 = \frac{3}{2(1.293)} \left[1 - \frac{1.293}{10.5(1.293) - 7.5} + \frac{1 - 1.293}{3.92(1.293)^2 - 1.4(1.293) - 1}\right] = 0.822 \ .$$

The theoretical sealing coefficient at $Re_c = 400$ becomes:

$$\Lambda_T = K_4 (4.50) + K_5 (7.23) = 0.639 (4.50) + 0.822 (7.23) = 8.81 \ .$$

Assume $Re_c = 1000$. Then

$$F_{\xi} = 0.00509 \left[2000 \cos 14.5 \left(\frac{1000}{317}\right)\right]^{0.746} = 3.36$$

and similarly,

$$F_{\eta} = 2.69 \ ,$$

from which,

$$K_4 = \frac{3}{2(3.36)} \left[1 - \frac{3.36}{10.5(3.36) - 7.5} + \frac{1 - 3.36}{3.92(3.36)^2 - 1.4(3.36) - 1}\right] = 0.365 \ ,$$

likewise

$$K_5 = 0.447 \ .$$

The theoretical sealing coefficient at $Re_c = 1000$ becomes:

$$\Lambda_T = K_4\ (4.50) + K_5\ (7.23) = 0.365\ (4.50) + 0.447\ (7.23) = 4.885\ .$$

These calculations are repeated for a number of assumed Reynolds numbers in the desired range of operation from which the theoretical performance curve may be drawn. A plot of such a curve is presented in Figure 14. A computer program is presented in Appendix B for the calculation of Λ_T as outlined above.

APPENDIX B

COMPUTER PROGRAM FOR THE SEALING COEFFICIENT

The computer program for Λ_T was written in Fortran IV and run on an I.B.M. 7040 computer. The terms in the program are related to the nomenclature utilized in this report as follows:

$A = I_1$	$E = I_3$	$P_5 = K_4$	$P_4 = K_5$
$B = I_2$	$F = I_4$	$P_1 = F_\xi$	$P_2 = F_\eta$

VISCO SEAL SEALING COEFFICIENT THEORETICAL Λ FOR LAMINAR AND TURBULENT OPERATION

```
1           REAL LAMBDA
2       98  FORMAT(//4X,1HC,14X,5HGAMMA,9X,5HALPHA,13X,4HBETA,13X,1HD/)
3       20  PRINT 98
4           RE=100.
5           DELRE=100.
6           READ 99,C,GAMMA,ALPHA,BETA,D
7           PRINT 95,C,GAMMA,ALPHA,BETA,D
10      99  FORMAT(5(F10.6))
11      95  FORMAT(5(F10.6,6X))
12          T=TAN(ALPHA/57.32)
13          A=(1.-GAMMA)*T**2
14          B=BETA**3*GAMMA*T**2
15          E=BETA**3/(GAMMA+BETA**3*(1.-GAMMA))
16          F=T*(1.-GAMMA+GAMMA*BETA-(GAMMA+BETA**3*(1.-GAMMA)+GAMMA*
            1(BETA-1.))/(GAMMA+BETA**3*(1.-GAMMA)))
17      97  FORMAT(12X,2HRE,13X,6HLAMBDA///)
20          REC=41.1*SQRT((D/2.)/((1.-GAMMA)*C+GAMMA*C*BETA))
21          PRINT 97
22          DO 10 I=1,30
23          IF((RE/REC)*COS(ALPHA/57.32)-.575)11,11,12
24      11  P5=1.
25          GO TO 13
26      12  P1=.00509*(2000.*(RE/REC)*COS(ALPHA/57.32))**.747
27          P5=(3./(2.*P1))*(1.-P1/(10.5*P1-7.5)+(1.-P1)/3.92*P1**2-1.4*P1
            1-1.))
30      13  IF((RE/REC)*SIN(ALPHA/57.32)-.225) 14,14,15
31      14  P4=1
32          GO TO 16
33      15  P2=.0101*(2000.*(RE/REC)*SIN(ALPHA/57.32))**.754
34          P4=(3./(2.*P2))*(1.-P2/(10.5*P2-7.5)+(1.-P2)/(3.92*P2**2-1.4*P2
            1-1.))
35      16  LAMBDA=P5*(A+B)/F+P4*E/F
36          PRINT 96,RE,LAMBDA
37      96  FORMAT(10X,F6.0,10X,F8.4)
40          IF(RE.GE.1000.) DELRE=400.
41      10  RE=RE+DELRE
42          GO TO 20
43          END
   $ENTRY
```